

# **Transaural Beamforming**

**Methods for Controllable Focused Sound Reproduction**

Markus Guldenschuh

# **Transaural Beamforming**

## **Methods for Controllable Focused Sound Reproduction**

Master's Thesis

at

Graz University of Technology

submitted by

**Markus Guldenschuh**

Institute of Electronic Music and Acoustics,  
University of Music and Performing Arts Graz  
A-8010 Graz, Austria

29<sup>th</sup> September 2009

© Copyright 2009 by Markus Guldenschuh

Supervisor: Univ.-Ass. DI Dr. Alois Sontacchi

Assessor: O.Univ.-Prof. Mag.art DI Dr.tech. Robert Höldrich



# **Transaurales Beamforming**

## **Methoden zur nachgeführten Schallfeldkonzentration**

Diplomarbeit

an der

Technischen Universität Graz

vorgelegt von

**Markus Guldenschuh**

Institut für Elektronische Musik und Akustik,  
Universität für Musik und darstellende Kunst Graz  
A-8010 Graz, Austria

29. September 2009

© Copyright 2009, Markus Guldenschuh

Diese Arbeit ist in englischer Sprache verfasst.

Betreuer: Univ.-Ass. DI Dr. Alois Sontacchi

Begutachter: O.Univ.-Prof. Mag.art DI Dr.tech. Robert Höldrich



## Abstract

In literature, several proposals can be found on how to synthesize or resynthesize sound fields. In general, there are two main strategies. Global approaches, like Wave Field Synthesis or Ambisonics, have been derived over physical equivalents and aim to reproduce a sound field within a whole area. Local approaches on the other hand, are designed to reproduce the sound field at the position of a user only, as for example with binaural signals via headphones.

The inherent goal of this work is to elaborate possible improvements for air traffic control communication conditions. In order to free air traffic controllers from the demanding usage of headphones, a loudspeaker array based application is introduced. The array produces binaural signals at the ears of the user to provide spatialized audio. It is therefore a local approach of sound source reproduction, that, however, suffers from unwanted cross talk from one binaural signal to the contralateral ear.

Different beamforming methods are investigated under the aspect of focusing quality, room excitation, dynamic adaptation and their contribution to an effective cross talk cancellation. It is a weighted Delay & sum Beamformer, a Least Squares Beamformer, a Maximum Energy Difference Beamformer and a Minimum Variance Distortionless Response Beamformer. The first method proved to be very feasible for its facile implementation. Although its principle is very easy, its results are comparable to the other methods that use optimization algorithms for the sound field manipulation.

Finally, a cross talk cancellation solution for a loudspeaker array and a binaural signals is deduced and the functionality of the overall system is underlined with measurements results.

## Kurzfassung

In der Literatur gibt es zahlreiche Ansätze und Vorschläge für die Synthese und Resynthese von Schallfeldern. Dabei lassen sich primär zwei unterschiedliche Strategien unterscheiden. Globale Ansätze wie Ambisonics oder die Wellenfeld Synthese, streben die Reproduktion eines Schallfeldes in einem größeren Areal an. Lokale Anwendungen hingegen, zielen darauf ab, das Schallfeld an der definierten Position einer Hörerin zu steuern. Dazu gehört beispielsweise die Wiedergabe binauraler Signale mit Kopfhörern.

Die Motivation dieser Arbeit war Verbesserungsmöglichkeiten für die akustische Kommunikationsschnittstelle von Fluglotsinnen zu erarbeiten. Um Fluglotsinnen vom anstrengenden, weil dauerhaftem, Gebrauch von Kopfhörern zu befreien, wird die Verwendung eines Lautsprecher Arrays vorgeschlagen. Der Lautsprecher Array soll binaurale, und damit spatialisierte, Signale an den Ohren der Nutzerin erzeugen. Es handelt sich deshalb um einen lokalen Ansatz zur Schallfeldreproduktion, der jedoch das Problem des Übersprechens von einem binauralen Signal zum kontralateralen Ohr mit sich bringt.

In dieser Arbeit werden verschiedene Methoden zur Schallfeldkonzentration untersucht. Die Methoden werden in Bezug auf ihre Fokussierungsqualität, ihre Raumanregung, ihre dynamische Steuerbarkeit und auf die Vorbedingungen für eine effektive Kanaltrennung verglichen. Im Speziellen werden ein gewichteter Delay & Sum Beamformer, ein Least Squares Beamformer, ein Maximum Energy Difference Beamformer und ein Minimum Variance Distortionless Response Beamformer verglichen. Im Vergleich stellt sich heraus, dass der Delay & Sum beamformer, dank seiner einfachen Implementierungsmöglichkeit, am geeignetsten für eine dynamische Echtzeitanwendung ist. Obwohl dem Delay & Sum Beamformer, im Gegensatz zu allen anderen Beamforming Ansätzen, kein Optimierungsalgorithmus zur Schallfeldproduktion unterliegt, sind seine Ergebnisse durchaus mit denen der anderen Beamforming Methoden vergleichbar.

Schlussendlich wird eine Übersprechkompensations-Lösung für einen Lautsprecher Array und ein Binauralsignal hergeleitet und die Funktionalität der Anwendung wird durch Messergebnisse gestützt.

## **Pledge of Integrity**

*I hereby certify that the work presented in this thesis is my own, that all work performed by others is appropriately declared and cited, and that no sources other than those listed were used.*

Place: \_\_\_\_\_

Date: \_\_\_\_\_

Signature: \_\_\_\_\_

## **Eidesstattliche Erklärung**

*Ich versichere ehrenwörtlich, dass ich diese Arbeit selbständig verfasst habe, dass sämtliche Arbeiten von Anderen entsprechend gekennzeichnet und mit Quellenangaben versehen sind, und dass ich keine anderen als die angegebenen Quellen benutzt habe.*

Ort: \_\_\_\_\_

Datum: \_\_\_\_\_

Unterschrift: \_\_\_\_\_

# Contents

<b>Contents</b>	<b>ii</b>
<b>List of Figures</b>	<b>iv</b>
<b>List of Tables</b>	<b>v</b>
<b>Acknowledgements</b>	<b>vi</b>
<b>Credits</b>	<b>vii</b>
<b>1 Introduction</b>	<b>1</b>
1.1 Motivation . . . . .	1
1.2 Introduction to the Technique of Beamforming . . . . .	3
1.3 Introduction to the Technique of Transaural Stereo . . . . .	5
<b>2 Beamforming</b>	<b>8</b>
2.1 Space-Frequency Signal Processing . . . . .	9
2.2 Spatial Transmission Functions . . . . .	14
2.3 Weighted Delay & Sum Beamforming . . . . .	17
2.4 Least Squares Beamforming . . . . .	26
2.5 Maximum Energy Difference Beamforming . . . . .	29
2.6 Minimum Variance Distortionless Response Beamforming . . . . .	31
2.7 Comparison of the Introduced Beamforming Methods . . . . .	32
<b>3 Transaural Stereo</b>	<b>41</b>
3.1 Concept of Transaural Stereo for a Loudspeaker Array . . . . .	41
3.2 Cross Talk Cancellation Results . . . . .	45

<b>4</b>	<b>Resume and Outlook</b>	<b>49</b>
4.1	Resume . . . . .	49
4.2	Outlook . . . . .	50
<b>A</b>	<b>Notation</b>	<b>52</b>
<b>B</b>	<b>Comparison of the SPL Distribution of the Different Beamformers</b>	<b>53</b>
<b>C</b>	<b>XTC Frequency Responses</b>	<b>56</b>
	<b>Bibliography</b>	<b>61</b>



# List of Figures

1.1	Desktop integrable communication setup . . . . .	2
1.2	Block diagram of the developed transaural beamformer . . . . .	2
1.3	Smart antennas . . . . .	3
1.4	Time reversal mirror in a reverberating cavity . . . . .	4
1.5	Time reversal mirror with an exemplary impulse . . . . .	4
1.6	Head related transfer function . . . . .	5
2.1	Far field Delay & Sum beamforming . . . . .	8
2.2	Vibrating stripes in an infinite wall . . . . .	9
2.3	Sound particle velocity distribution and k space spectrum of vibrating stripes .	10
2.4	The k space spectrum as measure of directivity . . . . .	11
2.5	Window influence on the directivity pattern . . . . .	12
2.6	Influence of the membrane width on the k space spectrum and the directivity . .	13
2.7	Measurement setup . . . . .	15
2.8	Loudspeaker equalization filter . . . . .	16
2.9	Measurement frequency response . . . . .	16
2.10	Weighted Delay & Sum beamforming . . . . .	18
2.11	Broad band comparison: measurement - free field simulation . . . . .	18
2.12	Bark bands and focus positions for comparison 1 . . . . .	19
2.13	Bark band comparison: measurement - free field simulation . . . . .	20
2.14	Bark band comparison: (weighted) SPL differences. . . . .	20
2.15	Sound field error statistics . . . . .	21
2.16	Focusing quality in dependence of the focus position for a bent array. . . . .	23
2.17	Focusing differences between bent and straight array. . . . .	24
2.18	3D directivity of a straight and a bent array . . . . .	25
2.19	Broad-band Least Squares beam . . . . .	27

2.20	Frequency dependent focusing . . . . .	27
2.21	Broad-band Least Squares beam with frequency dependent focus area . . . . .	28
2.22	Broad band Maximum Energy Difference beam with driving functions . . . . .	30
2.23	Broad band Minimum Variance Distortionless Response beam . . . . .	32
2.24	Influence of SVD regularization on the condition number . . . . .	33
2.25	Least Squares beam with measured transfer functions . . . . .	34
2.26	LS and MVDR driving functions . . . . .	35
2.27	Impulse responses of the driving functions . . . . .	36
2.28	Influence of SVD regularization to the directivity . . . . .	37
2.29	White noise gain . . . . .	38
2.30	Frequency response at the focus point . . . . .	38
2.31	SPL decay reference point . . . . .	39
3.1	Channel separation due to beamforming I . . . . .	42
3.2	Channel separation due to beamforming II . . . . .	42
3.3	Transfer paths of the transaural beamformer . . . . .	43
3.4	Dynamic range of the cross talk canceler . . . . .	45
3.5	Channel separation with cross talk canceler . . . . .	46
3.6	Temporal behavior of the cross talk canceler. . . . .	46
3.7	Transaural beamforming quality. . . . .	48
B.1	Weighted delay & sum beam in 3 bands . . . . .	53
B.2	Least squares beam in 3 bands . . . . .	54
B.3	Least squares beam with SVD regularization in 3 bands . . . . .	54
B.4	Least squares beam with frequency dependent focus area in 3 bands . . . . .	54
B.5	Maximum energy difference beam in 3 bands . . . . .	55
B.6	Minimum variance distortionless response beam in 3 bands . . . . .	55
B.7	Minimum variance distortionless response beam with SVD regularization in 3 bands . . . . .	55
C.1	XTC frequency responses for the close head positions with 2 rotation angles. . . . .	57
C.2	XTC frequency responses for the rear head positions and 2 rotation angles. . . . .	58

# List of Tables

2.1 Comparison of the beamforming methods . . . . .	40
---	----

# Acknowledgements

I would like to thank Dr. Alois Sontacchi for his support and the opportunities he gave me. Thanks to Franz Zotter and Hannes Pommberger for discussion, explanations and advices, as well as to Sabrina Metz for assisting me during my measurements.

Special thanks to my family who always encouraged me in all my intentions and to Johanna for being there for me.

Markus Guldenschuh  
Graz, Austria, September 2009

# Credits

This work was supported in part by Eurocontrol under Research Grant Scheme - Graz, (08-120918-C). Thanks, at this part, to Horst Hering for his helpful remarks.

The application that has been developed during this thesis uses the '*binaural Ambisonics*' patch written by Thomas Musil and '*Watson*' a video head-tracking program that was developed and kindly provided by Louis-Philippe Morency.

# Chapter 1

## Introduction

### 1.1 Motivation

This thesis is the result of investigations that were initialized by a project supported in part by the 'Eurocontrol Research Grant'. The goal of the project is to develop an advanced communication setup for air traffic controllers. The improvements primarily should contain:

- A head set free communication setup, to free the air traffic controller from the demanding usage of headphones.
- A fully spatialized sound to be able to acoustically localize the communication partners.

It has to be considered that some dozens controllers work simultaneously in air traffic control (ATC) centers. That raises some problems, especially for the first point. If loudspeaker boxes should be used instead of headphones, the sound excitation of the room runs the risk to be more annoying than the usage of head sets. The strategy is therefore to produce a focused sound that is always steered to the position of the user. As the user moves within a certain area, the steering has to be dynamic and adaptive. A video system is suggested to track the position and rotation of the user.

The preconditions in air traffic control deliver two relevant design criteria:

1. The bandwidth in air traffic control reaches from 300 to 2500 Hz.
2. The system should be desktop integrable and processing efficient.

Out of these criteria, the array properties (like shape, size and number of loudspeakers) and the sound focusing method have to be deduced. A desktop integrated communication setup is suggested in Fig.1.1.

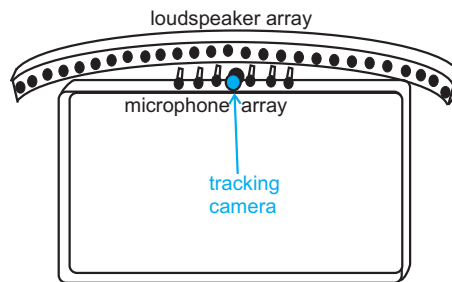


**Figure 1.1:** The loudspeaker- and microphone array, as well as the the USB camera for the user tracking can be mounted over the air traffic control screen in order to yield a compact system without any head worn hardware.

Fig.1.2 shows the block diagram of the overall system. Sound spatialization is accomplished through binaural signals, which are rendered in the binaural Ambisonics system. The 2-channel binaural signals are applied to a cross-talk canceler before they are led to the beamforming stage that produces a focused sound field. Both terms *beamforming* and *binaural signal* are explained

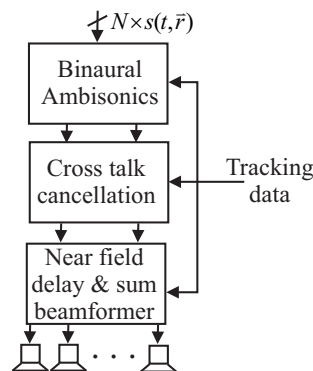


**Figure 1.2:** Arbitrary many sound sources can be rendered to a 2-channel binaural signal. The binaural signal runs through a cross talk cancellation filter before it is led to the beamformer.

in the following sections. The binaural Ambisonics system is not in the scope of this thesis as it is well described in Noisternig et al. [2003].

## 1.2 Introduction to the Technique of Beamforming

Beamforming has been used since the late 1970s as spatial filter in sensor technologies. A first overview was given by Veen and Buckley [1988]. An array of sensors has been used to filter electromagnetic or sonic waves from a certain direction. If several sensors are in a line in the direction of the incident wave with an interelementary distance of a multiple of the wavelength, the arriving wave is in phase on every sensor. Thus the signal can be amplified by constructive addition. In telecommunications, this principle is called smart antenna. (See Fig.1.3.) An

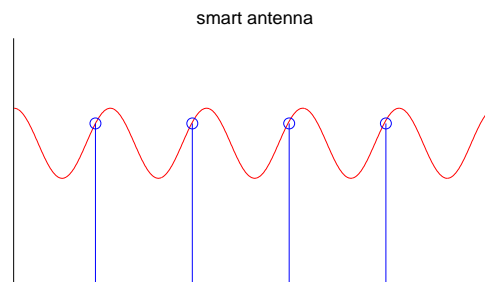


**Figure 1.3:** The concept of smart antennas: An array of sensors samples a wave in the distance of a wavelength.

extensive collection of beamforming methods for microphone arrays is given by Brandstein and Ward [2001]. Due to the tight relation to loudspeaker arrays, these methods can also be applied to calculate the driving function of the loudspeakers to produce a steered sound beam.

In this thesis, the Weighted Delay & Sum Beamformer, the Least Squares Beamformer, the Maximum Energy Difference Beamformer and the Minimum Variance Distortionless Response Beamformer are examined. The first is the physical straight forward method. It emphasizes the waves for a certain direction by simple constructive superposition without frequency dependent filtering. All other examined beamforming methods are so called super directive beamformers; meaning that they achieve a higher directivity than the simple delay & sum beamformer by additional filtering in the frequency domain.

If a sound pressure concentration in a certain point is desired, like it is the case in this thesis, there exists an other straight physical method to achieve a super resolution. This method is called time reversal mirror and it makes use of room reflections. In Yon et al. [2003], the principle of the time reversal mirror is explained over a reverberating cavity that, in a first step, is closed by an array of microphones like it is shown in fig. 1.4. At some point in this cavity a pulse is emitted. If the signals recorded by the microphones are played back time inverted<sup>1</sup>, the sound propagates back and focuses on the initial emitter point. A schematic impulse response with a direct wavefront and reflections is drawn in Fig.1.5. These reflexions will appear as

<sup>1</sup>Whereby the microphones are replaced by loudspeakers with identical spatial properties. (I.e. the spatial sensitivity of the microphones corresponds with the spatial radiation pattern of the loudspeakers.)



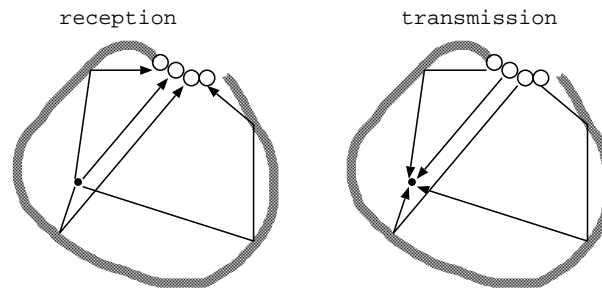


**Figure 1.4:** The reverberating cavity is closed by microphones in a first step. The microphones record a direct pulse with all its reflections. In a second step, the cavity is close with loudspeakers that play back the microphone signals time reversed. The reflections and the direct pulse gather in the original source point where they cause a super resolution. (Adapted from Yon et al. [2003])

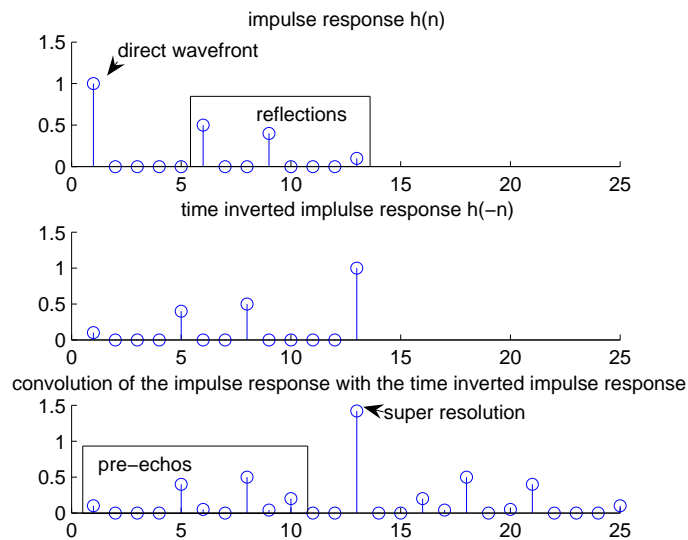


**Figure 1.5:** The upper figure schematizes the impulse response of one microphone and the middle is its time inverted version. In acoustics, source and sink can be repaced<sup>1</sup>. Thus, the impulse response also counts for the path from the loudspeakers back to the original emitting point. If the time inverted impulse is sent back (which is being convolved with the original impulse response), the reflections and the direct part superpose to a super resolution impulse (lower figure). However with the cost of pre-echos, caused by the time inverted signal.

pre-echos, when played back time inverted. On the other hand, after having run through the reflection paths again,<sup>2</sup> they are also constructively added with the directional part. This results in a main impulse that is even stronger than the original first wavefront has been. That is why it is called super resolution. On the one hand, the reflections help to focus the sound into a specific point, but on the other hand, they cause pre-echos that are disturbing especially for plosive sounds (Yon et al. [2003]). An adaptive system that is able to follow a moving user needs to know all the impulse responses of the area in which the user can move. To cover one

<sup>2</sup>I.e. a convolution with the original impulse response.

square meter only, approximately 210 impulse responses would have to be determined<sup>3</sup> which makes the time reversal mirror impractical for a facile implementation.

## 1.3 Introduction to the Technique of Transaural Stereo

### 1.3.1 Binaural Signals

Humans with normal hearing abilities can estimate the position of sound sources due to differences between the right ear signal and the left ear signal. This pair of ear signals is called binaural signal. Binaural signals and their influence on spatial hearing were investigated in Blauert [1999]. The most relevant differences between these signals are the interaural time difference (ITD) and the interaural intensity difference (IIDs). Additional coloration is caused by reflections from the shoulders and the pinna. All these differences are integrative parts of the head related transfer functions (HRTFs). Such a pair of HRTFs is depicted in Fig.1.6.

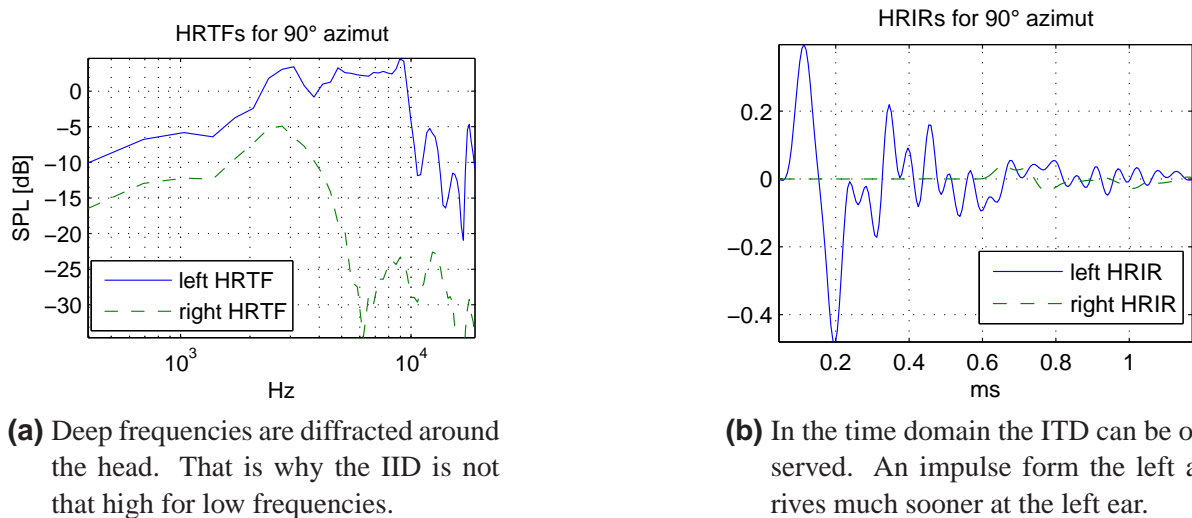


**Figure 1.6:** Head related transfer functions (HRTFs) and head related impulse response (HRIR) for 90° azimuth and 0° elevation.

As HRTFs depend on the shape of the ear and the torso geometry, they exhibit a unique profile for every human. Still, a good average HRTF can be won with measurements on dummy heads. The measurement of HRTFs is well described in Moller et al. [1995], while Algazi et al. [2001] investigated the capabilities of modeling HRTFs analytically.

HRTFs can be used to spatialize sound. If a mono source is convolved with a pair of HRTFs, the resulting binaural signal evokes a spatial impression, if each channel is led directly to the ears. The most common way to perceive binaural signals is thus via headphones. If binaural

<sup>3</sup>The minimal spatial resolution will be a topic of section 2.1.

signals are wanted to be played back via loudspeaker boxes, the technique of transaural stereo has to be applied.

### 1.3.2 Transaural Stereo

The playback of binaural signals via loudspeaker boxes causes an unwanted cross talk from the left binaural signal to the right ear and vice versa. With the knowledge of the HRTFs from the loudspeakers to the ears, these cross talk paths can be reduced. A first filter solution for cross-talk cancellation was derived by Atal and Schroeder [1963]. Bauck and Cooper [1996] showed solutions for cross talk cancellation (XTC) filters for various constellations of loudspeakers, listeners and binaural signals. A first binaural sound system for loudspeakers and tracked users has been developed by Gardner [1997]. Lentz [2006] investigated the stability of the XTC filters for 2 loudspeakers in dependence of their opening angles. It resulted that an opening angle of  $90^\circ$  delivers satisfying results. As a consequence, a set of 4 loudspeakers was placed every  $90^\circ$  around the user, to guarantee stable cross talk filters for a full rotation of the user. Of course, the functionality of XTC depends on the accuracy of the HRTFs. Firstly, it is the closeness to the actual personal HRTFs and secondly it is the dependency on the precision of the tracking system. Bai et al. [2005] tried to gain robustness against lateral mismatches by applying a crosstalk network from 6 loudspeakers to 6 control points (instead of to 2 ear positions only).

A first transaural system with focused sound was introduced by Menzel et al. [2005] and maintained by Laumann et al. [2008]. They used a circular array of 22 loudspeakers that produces virtual sound sources via Wave Field Synthesis (WFS). The virtual sound sources are chosen to be point sources. They are placed above the listener and play a binaural signal. Focused sound (like it is a point source, too) has the advantage that it causes less cross talk, if the focus spots are set in the vicinity of the ears. Laumann et al. [2008] took the HRTFs from the virtual point sources to the user for the XTC filters. The idea is, to rotate the virtual sound sources with the user, such that the same set of XTC filters can be used for any head rotation. However, it is not clear which benefit WFS contributes to the application and why the virtual sound sources are not set into the horizontal plane of the ears.

The goal of this thesis is to investigate different sound focusing methods and their feasibility to a dynamic transaural system with a tolerance to both, lateral movements and head rotations of the user. The investigations concern the directivity of the beamforming methods (and as a consequence their room excitation), their complexity in terms of a DSP realization, and the precondition for a stable cross talk cancellation. Section 2.1 gives a theoretical overview of spatial filtering before the different beamforming methods are described in section 2.3 to 2.6. For the simulations of the beamforming methods, the loudspeakers were assumed to be point sources. Measurements with real loudspeakers proved the concept and justify the simulations. In chapter 3 the calculation of XTC filters for 16 loudspeakers are deduced and the stability

of the XTC filters is discussed. The results of the performance of the transaural beamformer are presented before chapter 4 gives a resume of the thesis and an outlook to interesting future questions and ideas. The used vector- and matrix notation and the physical nomenclature is listed in appendix A.

# Chapter 2

## Beamforming

Beamformers use an array of transducers (such as antennas, microphones or loudspeakers) to steer into a certain direction or into a certain point of a wave field. The steering in general is achieved by filtering and summing up the signals of the different array elements. In the most trivial case, the signals are simply delayed and summed (Delay & Sum beamformer, see Fig. 2.1) such that they superpose constructively for a certain propagation direction or in a certain point. Beamforming can be done on the reception side (e.g. with microphones) or on the transmitting side. In this work, all discussion is done for beamforming with loudspeaker arrays, but due to the invertibility of acoustical paths, the following theory is valid for either case.

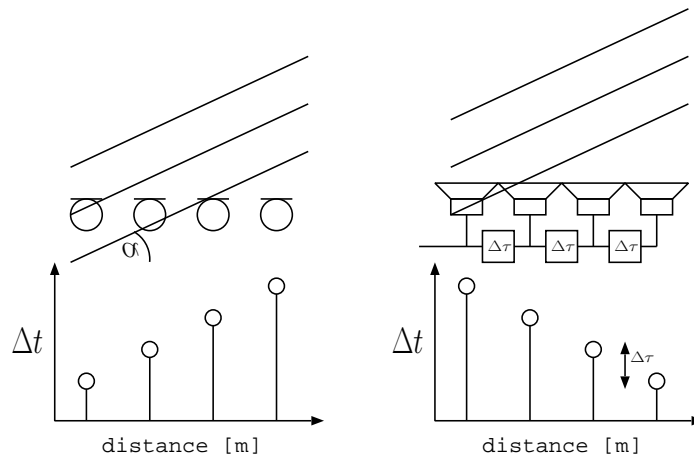


**Figure 2.1:** Recording and reproduction of an incident wavefront with a simple Delay & Sum beamformer.

In order to better understand the properties and limitations of beamformers, the next section throws a glance at the spatial Fourier transform before different beamforming methods are explained and investigated in detail.

## 2.1 Space-Frequency Signal Processing

To deduce the properties and limitations of beamformers, let us first consider an infinite wall with in phase vibrating stripes, as it is depicted in Fig.2.2. In Möser [1988] it is shown that

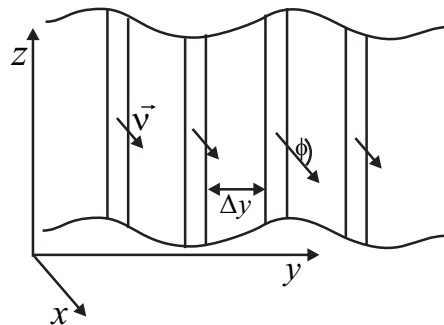


**Figure 2.2:** Stripes in an infinite wall that vibrate with a sound particle velocity  $nu$  into the orthogonal direction.

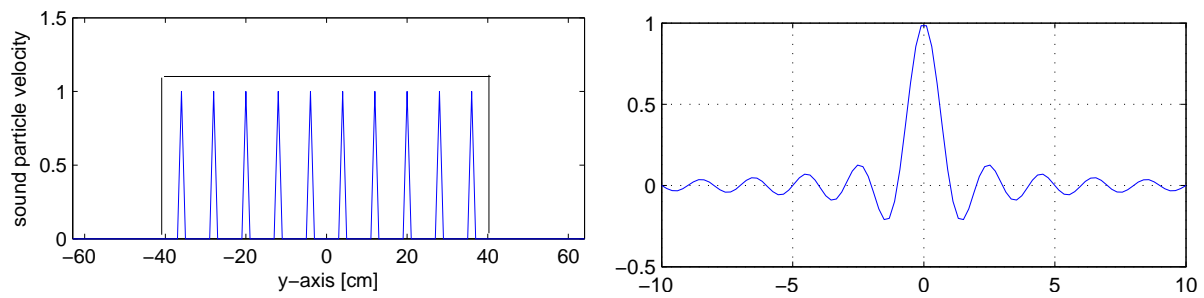
the directivity along the  $y$ -axis of these vibrating stripes in the far field can be derived over the Fourier integral over the sound particle velocity  $\nu_y$  along the very same axis

$$\Phi(k_y) = \int \nu(y) e^{-ik_y y} dy, \quad (2.1)$$

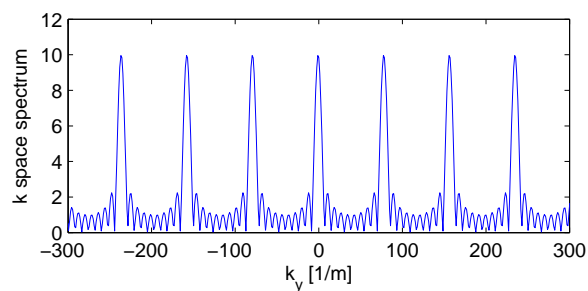
with  $k_y$  being the wavenumber in  $y$  direction.

$$k_y = \frac{\omega}{c} \sin(\phi). \quad (2.2)$$

Let us first consider the stripes as infinitesimally thin. Then, the sound particle velocity  $\nu$  can be expressed as an infinite pulse train along the  $y$ -axis for there is only sound particle velocity at the positions of the stripes (See also Williams [1999].) As known from time-frequency processing (Oppenheim [1989]), a pulse train stays unchanged through a Fourier transform. However, real arrays of course are not infinite. The finite length of the array can be described by a windowed version of our infinite pulse train (Fig.2.3a). The multiplication with a rectangle window corresponds to a convolution with a sinc function in the  $k$  space (Fig. 2.3c). The sinc function  $\text{sinc}(x) = \frac{\sin(\pi x)}{\pi x}$  (also shown in Fig.2.3b) has a main lobe around  $x = 0$  and descending side lobes that approximate zero in infinity.



- (a) There is only sound particle velocity at the discrete positions of the vibrating stripes. Hence, the sound particle velocity distribution can be described as a windowed pulse train.
- (b) The sinc function is the Fourier transform of a rectangle window.



- (c) In the k space the pulse train stays infinite but the pulses are convolved with the sinc function.

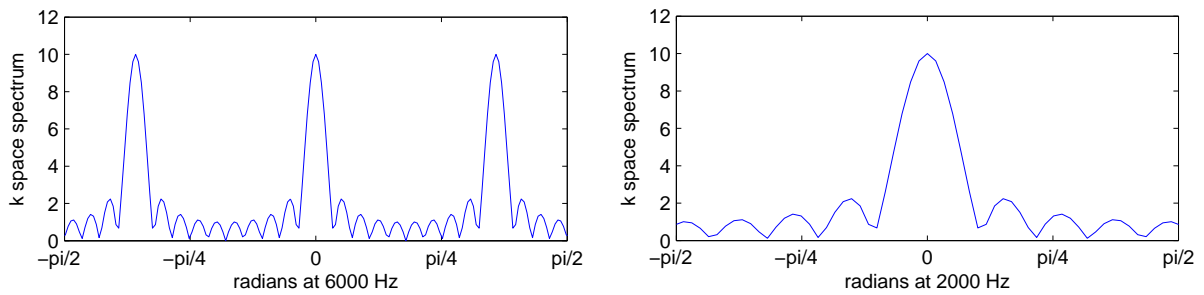
**Figure 2.3:** Sound particle velocity distribution of vibrating stripes along the y-axis and its spatial Fourier representation.

At a given speed of sound and a certain frequency,  $k_y$  only depends on  $\phi$ . Thus, the k space can be evaluated for every frequency form  $-\frac{\pi}{2}$  to  $\frac{\pi}{2}$ , which delivers a measure of directivity from  $-90^\circ$  to  $90^\circ$ . The lower the wavenumber, the less main lobes of the sinc function stay in the evaluated window from from  $-90^\circ$  to  $90^\circ$ . Spatial aliasing occurs as long as there is more than one main lobe in the evaluation window. Just as in time-frequency processing, the Nyquist theorem can be applied to the spatial domain, too. Spatial aliasing can be prevented as long as

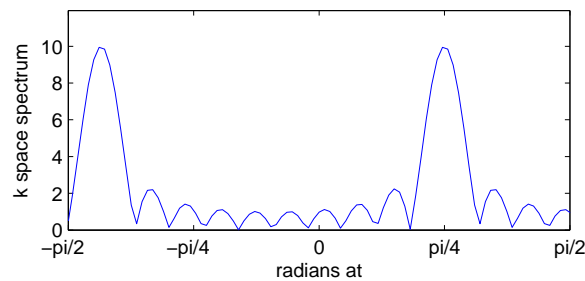
$$\frac{\lambda}{2} \geq \Delta y, \quad (2.3)$$

where  $\Delta y$  is the distance between the vibrating stripes.

Fig.2.4 shows the evaluation for 2 different frequencies. The k space spectrum was derived form Fig.2.3a which has an interelementary piston spacing of 8 cm. According to eq.(2.3), spatial aliasing occurs at 6000 Hz but not at 2000 Hz. Spatial aliasing can be prevented for higher frequencies by decreasing the distance between the array elements. Again, this can be explained by signal theory as in Oppenheim [1989]: A narrower pulse train of sound particle velocity leads to a wider pulse train after Fourier transformation. Hence, there are less main lobes in one period of the k space domain.



- (a)** At 6000 Hz, there are still 3 main lobes in the evaluation window form  $-90^\circ$  to  $90^\circ$ . Hence, there is spatial aliasing as the array radiates equally strong into 3 different directions. (Not forgetting that the radiation is equal on the back side of the wall.)
- (b)** At 2000 Hz, only 1 main lobe stays in the evaluation window. The array only radiates into the perpendicular ( $0^\circ$ ) direction. The spatial aliasing theorem of eq. (2.3) is fulfilled.



- (c)** First aliasing components appear, if the beam is steered to the side, like in this case for a frequency slightly over the Nyquist frequency with a steering angle  $\phi = -80^\circ$ .

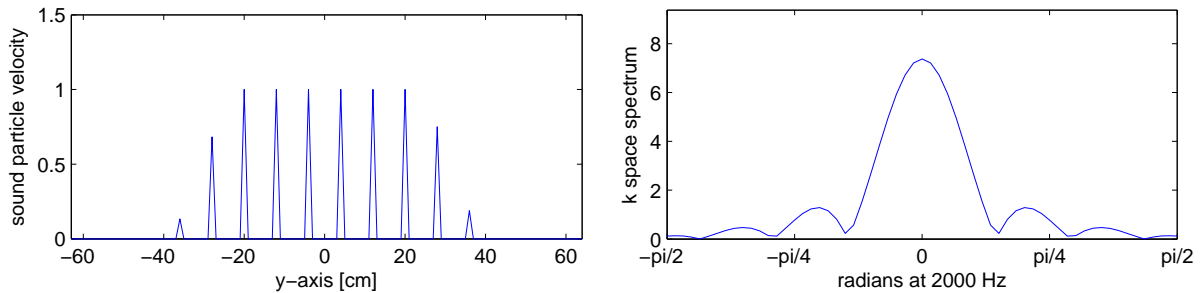
**Figure 2.4:** For a particular frequency and a given speed of sound, the k space spectrum only depends on  $\alpha$  and can be evaluated form  $-\frac{\pi}{2}$  to  $\frac{\pi}{2}$  or from  $-90^\circ$  to  $90^\circ$ , respectively. It can then be read as a directivity diagram.

The bandwidth in ATC reaches from 300 to 2500 Hz. This is a benefit for a loudspeaker array application, because spatial aliasing can mostly be avoided if the distance between the loudspeakers  $\Delta x$  does not exceed 7 cm. If the beam are steered to the side, however, aliasing can still occur. The beam is steered to an arbitrary direction  $\alpha$  through the delay times between the loudspeakers. This is also schematized in Fig.2.1. The delay times cause a linear phase shift  $e^{jk_y y \alpha}$  of the sound particle velocity that modulates the main lobe towards the steering angle  $\alpha$ . As a consequence, ambiguous main lobes might move into the evaluated directivity diagram, which is the case in Fig. 2.4c.

Comparing Fig.2.4a and 2.4b also shows that the beam width depends on the frequency. The beam width is defined by the -3 dB decay of the beam. The smaller the wavelength, the smaller is the beam width. However, the narrowness of the beam is limited by  $\frac{\lambda}{2}$  as described in Yon et al. [2003]. The second influence on the beam width is the spatial window. The spatial window determines the length of the array and how the loudspeakers are faded out at the end



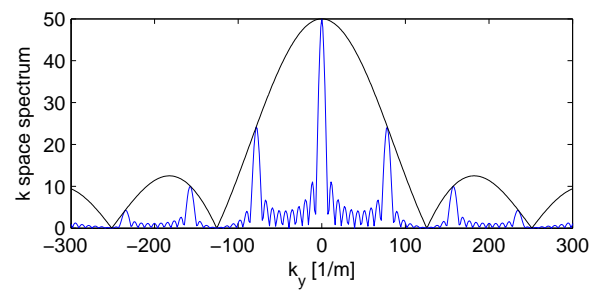
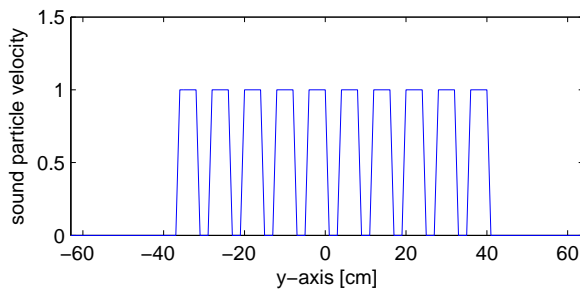
positions. A shorter array (a shorter spatial window) causes a broader directivity pattern and vice versa. A smoother window (instead of the hard rectangle limitation of Fig.2.3a) causes less side lobes, but widens up the main lobe, too, like it can be seen in Fig.2.5.



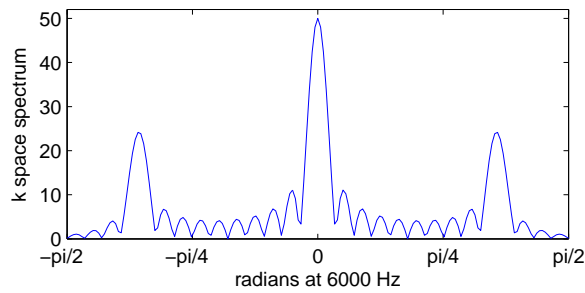
- (a) The gains of the loudspeakers towards the ends of the array are smoothly reduced to zero by a Hann window. (b) Compared to the rectangle window in Fig. 2.4b, the Hann window causes smaller side lobes but a wider main lobe.

**Figure 2.5:** A Hann window over the array elements compresses the side lobes but increases the width of the main lobe.

Until now, we considered the vibrating stripes to be infinitesimally small. That is why we could model the sound particle velocity distribution as pulse train. The real stripes of Fig.2.2 will have a sound particle velocity that looks like the rectangles in Fig.2.6a. This can be seen as a convolution of the pulse train with a rectangle window that has the width of the stripes. A convolution in the spatial domain corresponds to a multiplication in the k space, whereas a rectangle window changes to a sinc function through the Fourier transform. The result can be seen in Fig.2.6c. The pulse in the center of the k space (at  $k_y = 0$ ) is in the main lobe, while the other pulses will be more or less suppressed by the side lobes of the sinc function. The array loses its omnidirectionality, especially for high frequencies. This illustrates the fact, that a loudspeaker can only be considered as a point source, as long as the wavelengths are larger than the membrane diameter.



- (a) The width of the vibrating stripes determines the width of the rectangles in the  $\nu$  distribution along the  $y$ -axis. Again, there is only sound particle velocity at the position of the vibrating stripes. This  $\nu$  distribution can be interpreted as a convolution of the pulse train with a rectangle window.
- (b) The convolution with a rectangle in the spatial domain comes equal to a multiplication with a sinc window in the  $k$  space.



- (c) As a consequence, the directivity of the array is not omnidirectional any more.

**Figure 2.6:** The influence the membrane width on the  $k$  space spectrum and the directivity of the array.

## 2.2 Spatial Transmission Functions

### 2.2.1 Free field Green's Functions

The sound pressure of a sound source at an arbitrary observation point can be predicted with the help of Green's function. The free field Green's function relates the pressure at source point  $\mathbf{r}'$  to the pressure at an observation point  $\mathbf{r}$  for ideal conditions. Which are: omnidirectional point sources, no reflections, lossless medium etc. It is then the solution of the Helmholtz equation for outgoing spherical waves as in Morse [1953]

$$G(\mathbf{r}'|\mathbf{r}|\omega) = \frac{e^{-jk|\mathbf{r}'-\mathbf{r}|}}{|\mathbf{r}'-\mathbf{r}|}. \quad (2.4)$$

The Green's functions from all loudspeaker positions of an array  $\mathbf{r}'_1 \dots \mathbf{r}'_L$  to one specific focus point  $\mathbf{r}_f$  can be gathered to a vector

$$\mathbf{h}(\omega) = \left[ G(\mathbf{r}'_1|\mathbf{r}_f|\omega) \quad G(\mathbf{r}'_2|\mathbf{r}_f|\omega) \quad \dots \quad G(\mathbf{r}'_L|\mathbf{r}_f|\omega) \right]^T. \quad (2.5)$$

The sound pressure in the focus point  $p_{\text{focus}}$  can easily be calculated if the complex weights  $\mathbf{q}(\omega)$  of the loudspeakers (it is their amplitude and phase) are known

$$p_f(\omega) = \mathbf{h}^T(\omega) \mathbf{q}(\omega). \quad (2.6)$$

Equally,  $N$  arbitrary other field points can be considered as observation or evaluation points. The Green's functions from every source point  $\mathbf{r}'_l$  to every evaluation point  $\mathbf{r}_n$  are gathered in the matrix

$$\mathbf{G}(\omega) = \begin{pmatrix} G(\mathbf{r}'_1|\mathbf{r}_1|\omega) & G(\mathbf{r}'_2|\mathbf{r}_1|\omega) & \dots & G(\mathbf{r}'_L|\mathbf{r}_1|\omega) \\ G(\mathbf{r}'_1|\mathbf{r}_2|\omega) & G(\mathbf{r}'_2|\mathbf{r}_2|\omega) & \dots & G(\mathbf{r}'_L|\mathbf{r}_2|\omega) \\ \vdots & \vdots & \ddots & \vdots \\ G(\mathbf{r}'_1|\mathbf{r}_N|\omega) & G(\mathbf{r}'_2|\mathbf{r}_N|\omega) & \dots & G(\mathbf{r}'_L|\mathbf{r}_N|\omega) \end{pmatrix}. \quad (2.7)$$

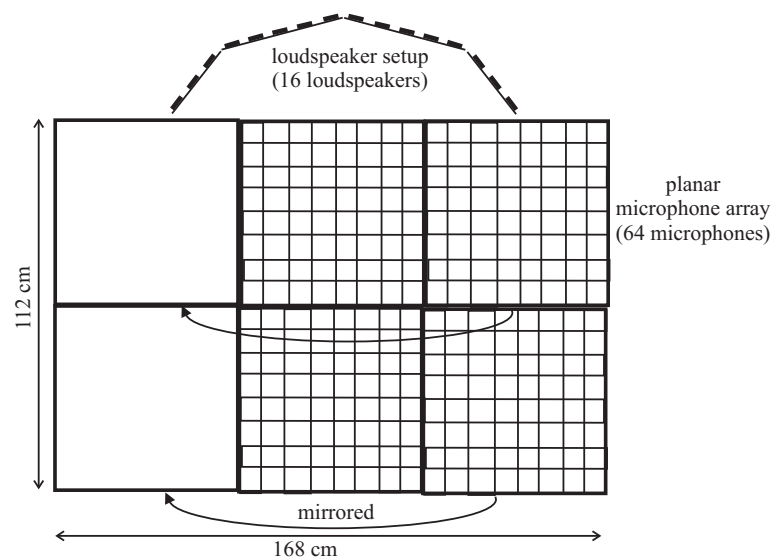
A multiplication of the source strength vector  $\mathbf{q}(\omega)$  with this matrix yields the sound pressure vector  $\mathbf{p}(\omega)$

$$\mathbf{p}(\omega) = \mathbf{G}(\omega)\mathbf{q}(\omega), \quad (2.8)$$

that contains the sound pressure in the  $N$  observation points  $\mathbf{r}_n$ . Thus the sound field of a beamformer with source strength vector  $\mathbf{q}(\omega)$  can be simulated with the knowledge of matrix  $\mathbf{G}(\omega)$ .

### 2.2.2 Transfer Functions Measurement

The free field Green's functions serve as theoretical background for simulations. In order to evaluate a real beamformer, the transfer functions from an experimental loudspeaker setup to 256 field points were measured, too. The loudspeaker array has to satisfy the spatial Nyquist theorem (eq. (2.3)) and requires a width of 120 cm to cover the working area of air traffic controllers. These constraints have led to an array of 16 loudspeakers that are arranged to approximate an elliptical segment. This constellation proofed to bear focusing advantages over a straight array, as it can be read in section 2.3.2 and in Guldenschuh et al. [2008]. A quadratic microphone array with a raster of  $7 \times 7$  cm was used to prevent spatial aliasing up to 2500 Hz. The measurement setup is depicted in Fig. 2.7.



- (a) The planar array of  $8 \times 8$  microphones was used in 4 positions. As we assume symmetry, the outer positions were mirrored to the other side. This finally leads to 384 evaluation points.



(b) Loudspeaker array with measurement microphones.

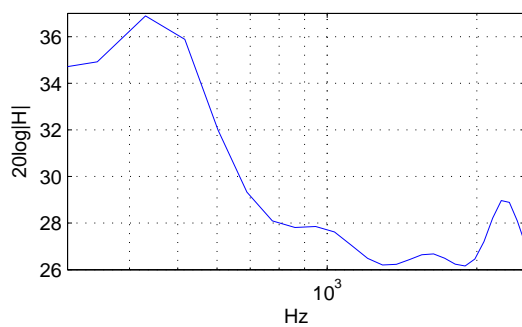
**Figure 2.7:** Measurement setup

The impulse responses were measured in a bandwidth from 300 to 2500 Hz with exponential sweeps as in Farina [2000]. The sweeps had a length of 2 seconds and were recorded with

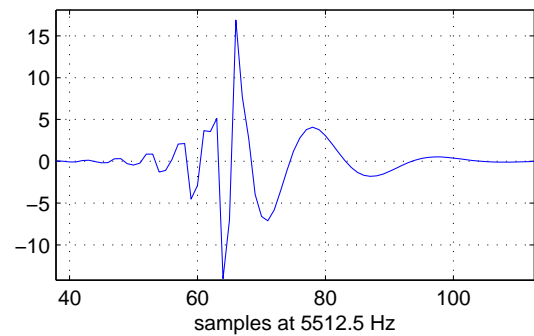
44.1 kHz sampling frequency. In order to consider the influence of the loudspeakers and microphones, a reference measurement of all loudspeakers in one meter distance was used to equalize the sound field measurement. In the frequency domain, the equalization can be done by inverse filtering

$$H_{\text{measure.eq}} = H_{\text{measure}} H_{\text{ref}}^{-1}. \quad (2.9)$$

An equalization filter  $H_{\text{ref}}^{-1}$  is shown in Fig.2.8.



**(a)** Frequency response of the inverse of  $H_{\text{ref}}$ . The used loudspeakers have a high pass characteristic. Therefore the equalization filter has to augment the basses.



**(b)** In the time domain, the inverse of  $H_{\text{ref}}$  has 60 taps at 5512.5 Hz sampling frequency.

**Figure 2.8:** Loudspeaker equalization filter in the frequency- and the time domain.

Unfortunately, early reflections from the microphone mounting device caused a comb filter that has its first notch around 2000 Hz. A sample of measured transfer functions can be seen in Fig.2.9. Finally, the impulse responses were resampled at a 8 times lower rate and their length

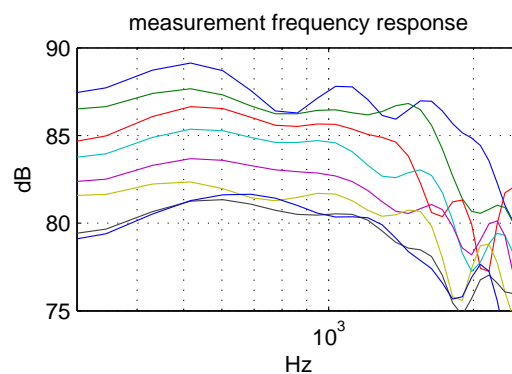


**Figure 2.9:** Frequency response of the first 8 loudspeakers to a central position in 90 cm distance. Early reflections from the microphone mounting device around 1 ms cause a first notch at around 2000 Hz.

was reduced to 2.9 ms.

Sound pressure levels (SPL)  $L_p$  are derived by the mean value over the squared amplitude

of every frequency bin  $\xi$  within the desired bandwidth.

$$\bar{p}^2 = \frac{1}{33} \sum_{\xi=1}^{33} \|p(\xi)\|^2 \quad (2.10)$$

$$L_p = 10 \log \frac{\bar{p}^2}{p_0^2} \quad \text{with } p_0 = 20 \mu\text{Pa}. \quad (2.11)$$

In the following all sound field evaluations (also the free field simulations) were done at the sampling frequency of 5512.5 Hz with a resolution of 33 frequency bins. All sound field representations are normed by the sound pressure level in the focus point.

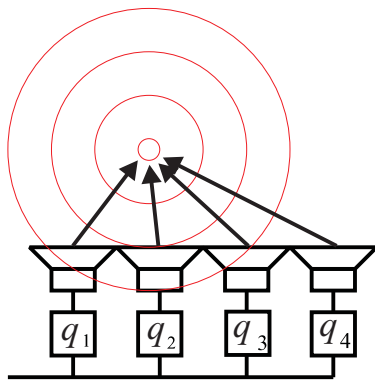
## 2.3 Weighted Delay & Sum Beamforming

To create a pressure concentration in a sound field, the signals of an array have to superpose constructively in the focus point. Hence, they have to reach the focus point at the same time. It follows that the source strength vector  $\mathbf{q}(\omega)$  has to be the complex conjugate of the Green's functions  $\mathbf{h}(\omega)$  (as defined in eq.(2.5)) to compensate for the phase differences of the Green's functions

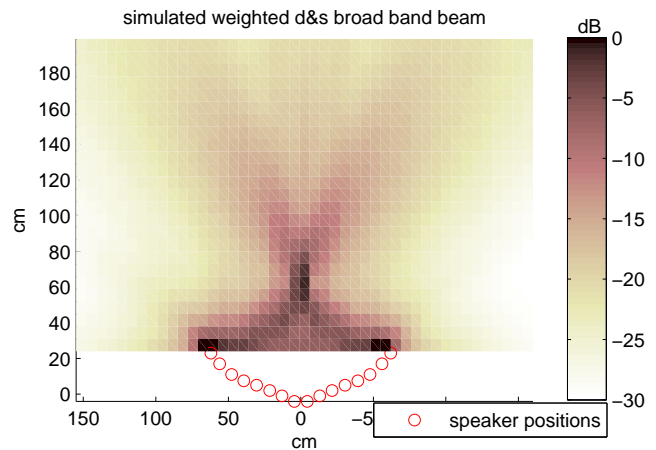
$$\mathbf{q}(\omega) = \mathbf{h}^*(\omega). \quad (2.12)$$

The Green's functions are weighted with the reciprocal of the distance from the loudspeaker to the focus point (see eq.(2.4)). Hence, the source strength vector  $\mathbf{q}(\omega)$  is weighted with this reciprocal, too. These weights can also be interpreted as a window that suppresses the loudspeakers that are further away from the focus point. Obviously, the frequency response or real loudspeakers has to be equalized to receive unity gain in the focus point. In contrast to the beamformer in Fig.2.1, the Weighted Delay & Sum beamformer (WDSB) (as any point focusing beamformer) has one individual complex weight per loudspeaker, like depicted in Fig.2.10a.

Cho and Roan [2009] pointed out that it would make sense to weight  $\mathbf{q}(\omega)$  with the reciprocal of the square or the cube of the distance, if the focus points are in the near field ( $kr < 2$ ). The lowest case of our application however, can be estimated as  $kr = 2.2$  with  $k = \frac{2\pi 300 \text{ Hz}}{c}$  and  $r = 0.4 \text{ m}$ . Therefore no attention has to be paid to near field weighting. Fig.2.10b shows a simulated beam in the bandwidth of 300-2500 Hz.



(a) Weighted delay & beamforming: Each loudspeaker has its own complex weight such that the waves superpose in the focus point.

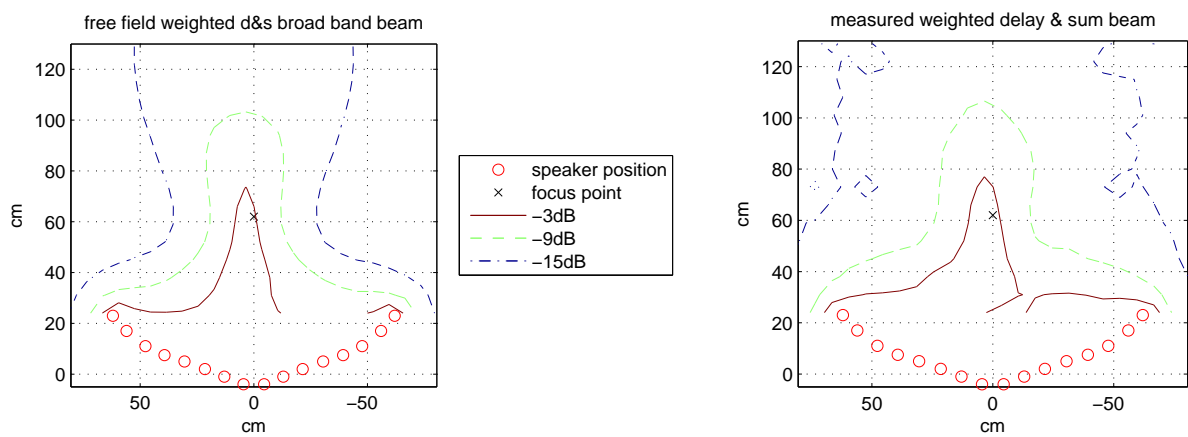


(b) Broad-band sound pressure distribution of a WDSB.

Figure 2.10: Weighted Delay & Sum beamforming.

### 2.3.1 Comparison 1: Measured Beam - Simulated Beam

The beams of the ideal free field Green’s functions were compared with the beams of the measured transfer functions. The first ones will be called simulated beams while the latter ones will be called measured beams from now on.<sup>1</sup> The broad band SPL distribution of a simulated and a measured beam are depicted in Fig.2.11. The comparison was done for 4 focus posi-



(a) Simulation, based on the free field Green’s functions.

(b) Simulation, based on the measured transfer functions.

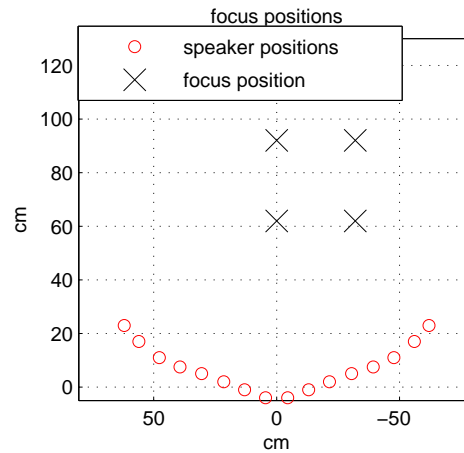
Figure 2.11: Comparison between the simulated and the measured beam in the close central position in the full bandwidth of 300-2500 Hz. The pressure decay is depicted in 3 level lines.

<sup>1</sup>Although the measured beams are simulated, too. But with data of the measured transfer functions.

tions (marked in Fig.2.12b), in 12 bark bands in the 384 evaluation points of Fig.2.7a. Bark bands simulate the frequency dependent sensitivity of the ear and are therefore also called critical bands. Their bandwidths were empirically determined by Zwicker [1990]. The used bark bands are listed in Table2.12a. The measurements shall proof the concept and justify further simulations based on the free field Green's functions.

bark	$f_l$	$f_u$
4	300	400
5	400	510
6	510	630
7	630	770
8	770	920
9	920	1080
10	1080	1270
11	1270	1480
12	1480	1720
13	1720	2000
14	2000	2320
15	2320	2700

(a) Lower and upper cut off frequencies of bark bands between 300 and 2700 Hz.



(b) The comparison between the beams of the measurement and the free field Green's functions was done for the marked 4 positions. As we assume symmetry of the sound field, all positions are chosen to be on the negative side of the x-axis.

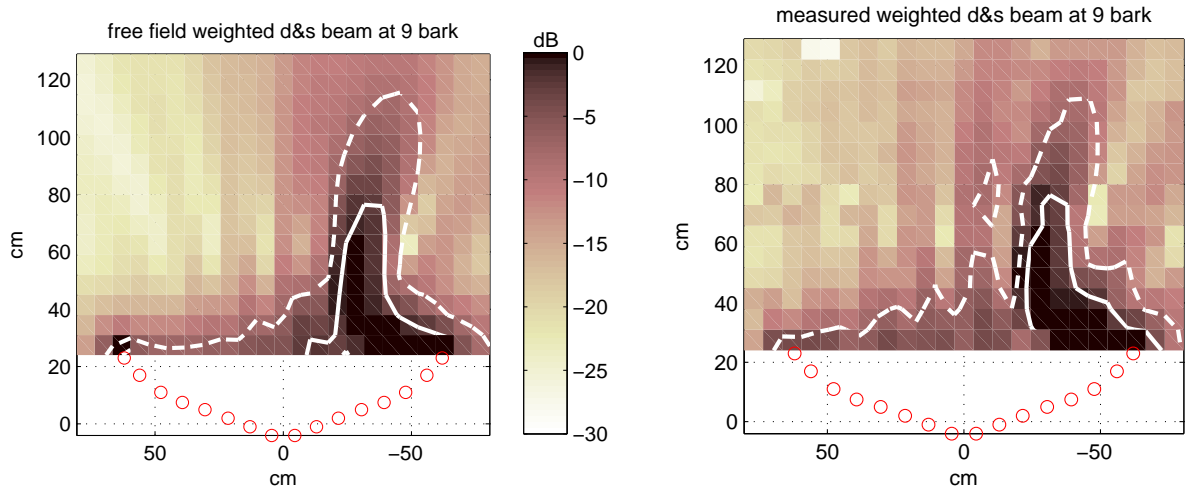
**Figure 2.12:** Bark bands and focus positions for the comparison between simulation and measurement.

Before the SPLs of the measured and the simulated sound field can be compared, the energy of the measured sound field  $\bar{p}_m^2$  has to be calibrated to the total energy of the simulated sound field.

$$\bar{p}_{m,cal}^2 = \bar{p}_m^2 \frac{\sum_{i=1}^{384} \bar{p}_{sim,i}^2}{\sum_{i=1}^{384} \bar{p}_{m,i}^2} \quad (2.13)$$

The comparison will exemplarily be shown at 9 bark for the close side position. The SPL distributions are shown in Fig.2.13, and the absolute value of their differences in Fig.2.14a. Errors outside of the focused area are less relevant, which is why we introduce a weighted difference  $e_w$ , too. The weights are the square root of  $p_{sim}$ , normed by the pressure in the focus





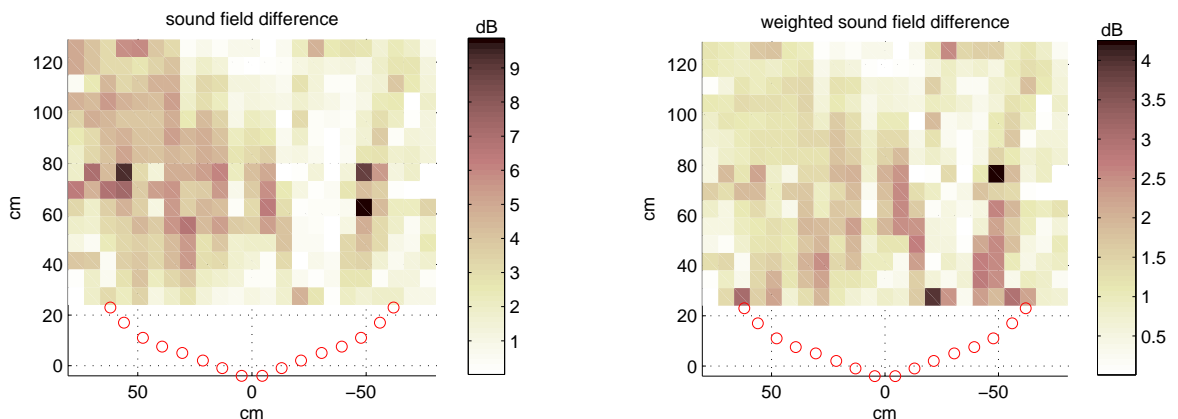
(a) Simulation, based on the free field Green's functions. (b) Simulation, based on the measured transfer functions.

**Figure 2.13:** Comparison between the simulated and the measured beam in the close side position in the 9<sup>th</sup> bark band. The solid white line represents the -3 dB level line and the dashed line the -9 dB level line.

point.

$$e_{w,i} = |L_{m,i} - L_{sim,i}| \sqrt{\frac{p_{sim,i}}{p_{focus}}} \quad (2.14)$$

As a consequence the error in the focus point stays the same, while errors in regions of low SPL are compressed. The weighted difference is shown in Fig.2.14b



(a) SPL differences in the close side position at 9 bark. The highest difference is 9 dB. (b) SPL differences, weighted with the square root of  $p_{sim}$ . Differences in regions of low SPL (like in the upper left corner) are suppressed. The highest difference is 4 dB.

**Figure 2.14:** SPL differences and weighted SPL differences between the measured and the simulated sound field in the 9<sup>th</sup> bark band.

The median and the mean value over all SPL differences and weighted differences are given in Fig.2.15. Mean and median of the weighted difference lie under 2 dB, which is a very satisfying result. Standard deviations, higher than 4 dB only occur for the unweighted difference and hence in regions of low SPL and minor interest. The measurement results give reason to the free field Green's functions simulations, which will therefore be used for further simulations.

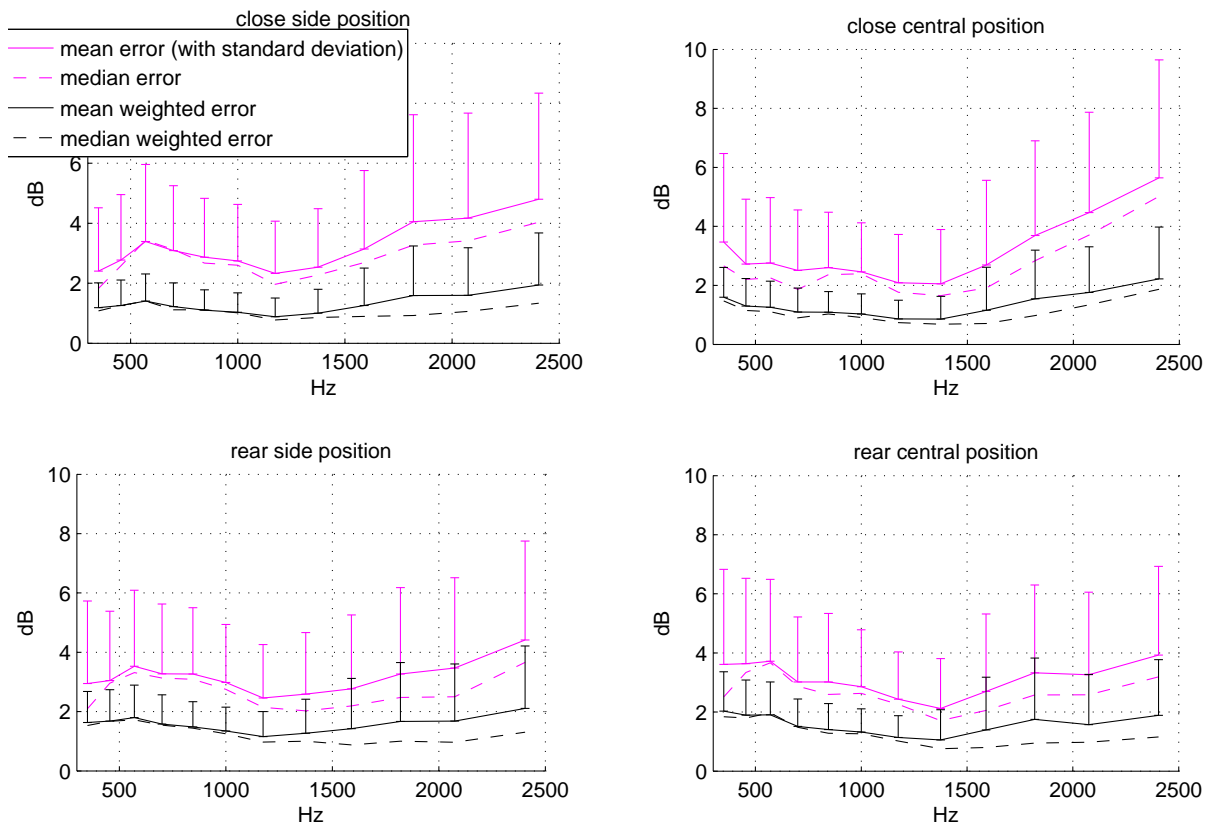


**Figure 2.15:** SPL difference and weighted difference between the measured and the simulated sound field for four focus positions. Differences are higher at high frequencies, where the areas of constructive and destructive superposition are smaller. A little phase error can then cause a constructive superposition at a location where the simulation predicts a destructive superposition, or vice versa. In addition frequencies around 2000 Hz suffer from the comb filter notch described in Fig.2.9.

### 2.3.2 Comparison 2: Straight Array - Bent Array

The sound focusing properties of parabolic and elliptical reflectors are well known in room acoustics like in Fasold [1998]. In the following, the focusing properties of a bent array will be compared to the ones of a straight array. Therefore, two measures are introduced.

1.  $\text{SNR}_{2D}$ : For the 2D comparison, the evaluation points of Fig.2.7a will be used. The  $\text{SNR}_{2D}$  is then the relation between the sound energy in the focus point to the average of the sound energy in all other 383 evaluation points in dB.

$$\text{SNR}_{2D} = 10 \log \left( 383 \frac{\bar{p}_{\text{focus}}^2}{\sum_i \bar{p}_i^2} \right) \quad (2.15)$$

2. Spatial rejection ratio (SRR): As SRR, we define the difference between the sound pressure level in the focus point and the sound pressure level of the reverberant room  $L_{\text{focus}} - L_r$ . In Ahnert [1993] it is shown that  $L_r$  can be estimated as

$$L_r = 10 \log \frac{P_{ac}}{P_0} - 10 \log A + 6 \text{ dB}, \quad (2.16)$$

where  $A$  is the sum of reflecting surfaces,  $P_0$  is the reference sound power of  $10^{-12}$  W and  $P_{ac}$  is the acoustic power of the array.  $P_{ac}$  is derived by integrating the sound intensity

$$\vec{I} = p\vec{v} \quad (2.17)$$

over the surface  $S$  of a sphere with radius  $r$ . If  $r$  is much greater than the array dimension  $l$

$$r \gg l, \quad (2.18)$$

$\vec{v}$  approximates the normal of the spherical surface for every loudspeaker in every point of the sphere. Thus,  $\vec{I}$  can be approximated as

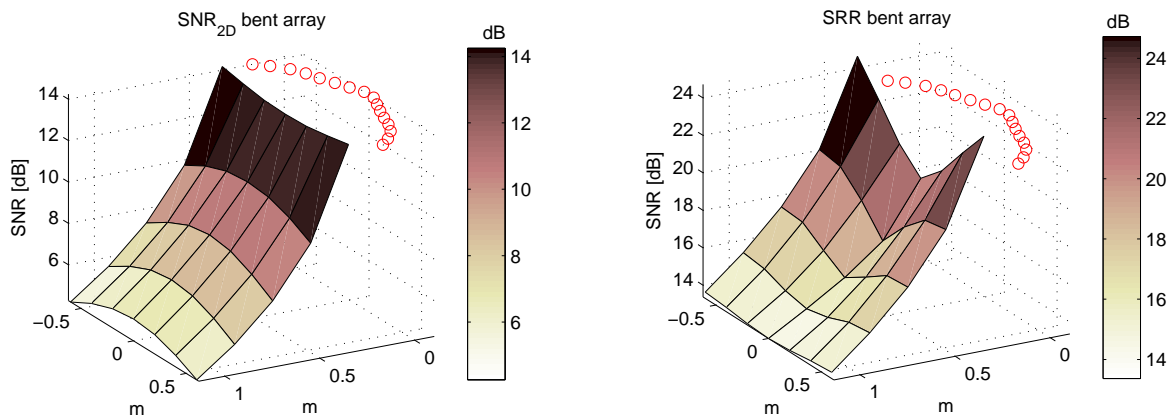
$$I = \frac{\bar{p}^2}{\rho c} \quad (2.19)$$

As the sound intensity is determined numerically, the integral has to be transformed to a sum over  $N$  discrete points

$$P_{ac} = \frac{1}{N} \sum_{n=1}^N \bar{p}_n^2 \frac{4\pi r^2}{\rho c}, \quad (2.20)$$

where  $\rho c$  is the acoustic impedance which has  $408 \frac{\text{kg}}{\text{m}^2\text{s}}$  at  $20^\circ\text{C}$ .

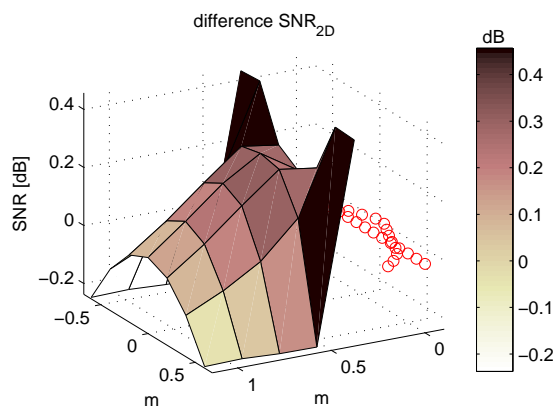
Simulations for 35 focus points are done to compare the two arrays. The centroids of the arrays are put into the coordinate origin and  $r$  is chosen to be 10 m to account for eq.(2.18). The sphere is sampled on  $N = 7482$  surface points to satisfy the spatial aliasing constraint of eq.(2.3) on a sphere with radius 1.7 m. This radius encloses the array and the farthest focus point. The results for the bent array can be seen in Fig.2.16, and the differences to the straight array ( $\text{SNR}_{\text{bent}} - \text{SNR}_{\text{straight}}$ ) are shown in Fig.2.17.



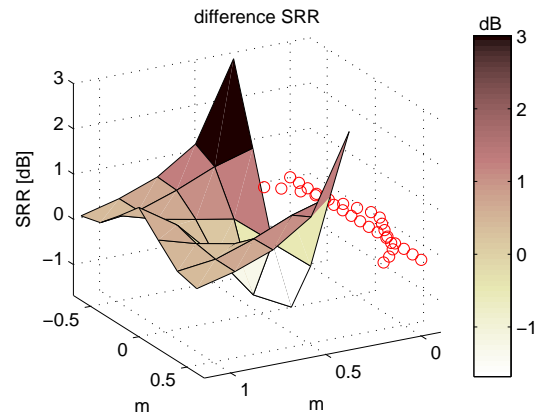
**(a)** Obviously the sound field is stronger excited if beam is steered further away from the array. As a consequence the  $\text{SNR}_{2D}$  decreases.

**(b)** Also the room is stronger excited, if the beam is steered further away. Remarkably is the notch for the close central focus positions. This effect will be explained later on.

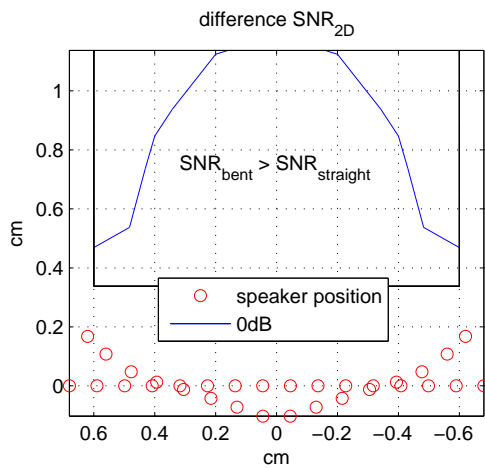
**Figure 2.16:**  $\text{SNR}_{2D}$  and SRR for 35 focus positions. Both measures decrease with the distance of the focus point from the array.



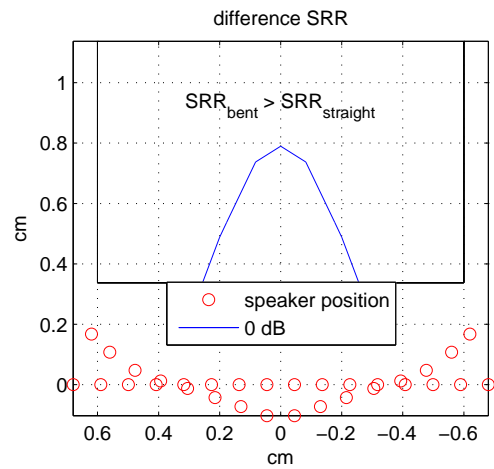
(a)  $SNR_{2D}$  differences between the bent and the straight array in 35 focus points. The differences are only marginal.



(b) The differences are slightly higher for the SRR.



(c) The 0 dB line marks the border where the bent array performs better in terms of the 2D SNR.



(d) In terms of the SRR, the bent array performs worse for close central focus positions. This effect is further investigated in Fig.2.18.

**Figure 2.17:** Focusing differences of a bent and a straight array. The bent array performs slightly better for both measures. The highest differences are reached for focus points in the near corners, where the bent array benefits from its closer position.

The most striking outcome is that the bent array performs worse for close central focus points, although we would assume (also by reason of the  $SNR_{2D}$  values) that focusing works more efficient, if the focus point is better surrounded by the loudspeakers. In the 2D case, this is true, but Keele [2003] pointed out that bent line arrays have a strong radiation orthogonal to their expansion plane. This effect can be seen in Fig.2.18. It can be concluded, that the

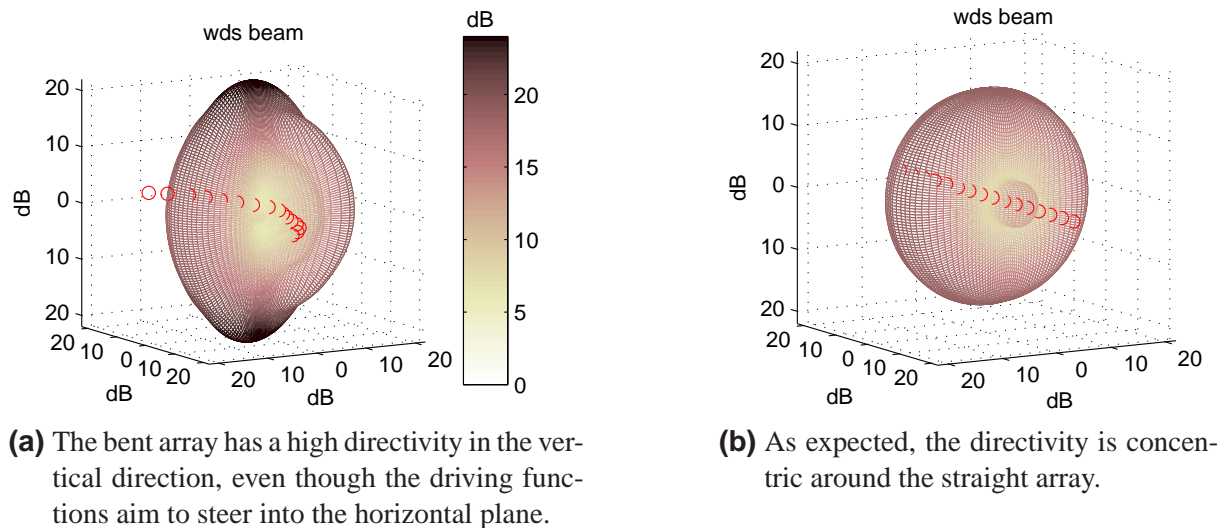


**Figure 2.18:** 3D directivity of a straight and a bent array for a close central focus point in the horizontal plane.

bent array has slightly better focusing properties than a straight array. Above all, the bent array performs better for focus positions in the close side positions, where it benefits from the close loudspeakers.

Weighted Delay & Sum beamforming is a physical straight forward beamforming method. It simply aims to focus sound in a specific point by compensating the delay times. Additional weights prevent loudspeakers from exciting the sound field too much, if they are further away from the focus point. A WDSB can therefore be realized very easily on a DSP. The input signals are led into a delay line and each output channel is weighted with one multiplier. This means that all frequencies are equally weighted and, as a consequence, the frequency response in the focus point is flat. Superdirective beamformers use optimization algorithms to narrow the beam width or to enforce regions of low SPL. In general, the amplitude and phase of their driving function is frequency dependent. So their implementation requires filtering. The following 3 sections introduce and investigate such superdirective beamformers.

## 2.4 Least Squares Beamforming

The Least Squares (LS) algorithm finds the source strength vector that causes an output (in our case a sound field) that matches a target function with the smallest (least) squared error. Our target function  $\tilde{\mathbf{p}}$  consists of  $p_{\text{focus}}$  and the sound pressure in  $N$  other field points

$$\tilde{\mathbf{p}}(\omega) = \begin{pmatrix} p_f \\ \mathbf{p} \end{pmatrix}. \quad (2.21)$$

Complementary, we combine the the Green's functions from the loudspeakers to the focus point with the Green's functions to the other  $N$  field points

$$\tilde{\mathbf{G}}(\omega) = \begin{bmatrix} \mathbf{h}^T \\ \mathbf{G} \end{bmatrix}. \quad (2.22)$$

The error between the target function and the outcome of the beamformer reads as

$$\mathbf{e} = \tilde{\mathbf{p}} - \tilde{\mathbf{G}}\mathbf{q}, \quad (2.23)$$

the squared error results in

$$e^2 = \mathbf{e}^H \mathbf{e} = \tilde{\mathbf{p}}^H \tilde{\mathbf{p}} - 2\mathbf{q}^H \tilde{\mathbf{G}}^H \tilde{\mathbf{p}} + \mathbf{q}^H \tilde{\mathbf{G}}^H \tilde{\mathbf{G}} \mathbf{q}. \quad (2.24)$$

The first derivative of  $e^2(\mathbf{q})$  describes the tangents of the error function. The tangent is flat (i.e.  $e^2 \frac{d}{d\mathbf{q}} = 0$ ) where  $e^2(\mathbf{q})$  has a minimum or a maximum. As the error function is quadratic and positive, the solution of the LS algorithm finds the minimum of the function. The derivative of  $e^2$  is

$$e^2 \frac{d}{d\mathbf{q}} \stackrel{!}{=} 0 \stackrel{!}{=} -2\tilde{\mathbf{G}}^H \tilde{\mathbf{p}} + 2\tilde{\mathbf{G}}^H \tilde{\mathbf{G}} \mathbf{q}, \quad (2.25)$$

and the Least Squares solution of the source strength vector is

$$\mathbf{q} = \left( \tilde{\mathbf{G}}^H \tilde{\mathbf{G}} \right)^{-1} \tilde{\mathbf{G}}^H \tilde{\mathbf{p}}. \quad (2.26)$$

From eq.(2.23) on, the dependency on  $\omega$  is omitted for reasons of compactness. In fact it is important that the LS solution has to be evaluated at every frequency. The stability of the LS filter depends on the number of considered frequency bins. However, the LS optimization for a limited number of frequency bins does not guarantee a flat frequency response in the focus point. This problem will be further discussed in section 2.7.

An example of a Least Squares beam (LSB) is depicted in Fig.2.19. The sound pressure is minimized within a frame around the arrangement This frame is meant to surround the working space of an air traffic controller. The chosen target function demands unity gain at the focus

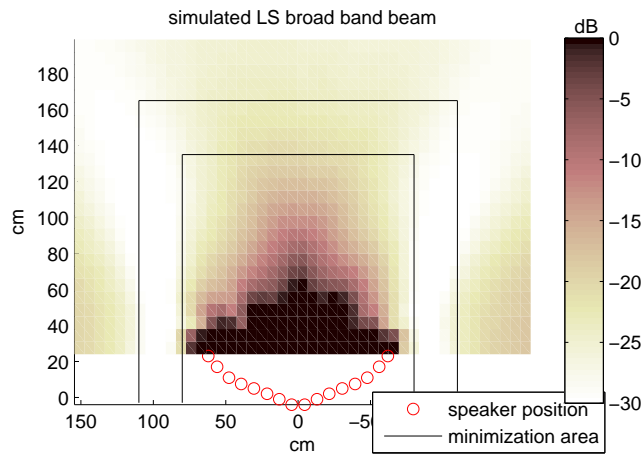


**Figure 2.19:** Broad-band (300-2500 Hz) sound pressure distribution of a LSB. The desired sound pressure is zero in the minimization area should be zero and has unity gain at the focus point.

point and zeros at all other control points

$$\mathbf{q} = (\tilde{\mathbf{G}}^H \tilde{\mathbf{G}})^{-1} \tilde{\mathbf{G}}^H \begin{bmatrix} 1 & 0 & 0 & \dots & 0 \end{bmatrix}^T. \quad (2.27)$$

For the targeted transaural application, the beams are aimed to be steered to the listener’s ears. On the one hand, this minimizes the radiated sound energy and on the other hand it reduces the cross talk. In chapter 3 it is explained that the cross talk increases with the wavelength. Therefore it would make sense to set the focus point dependent on the frequency. This is illustrated in Fig.2.20.

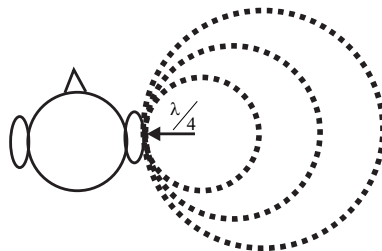


**Figure 2.20:** Several focus points can be located as a frequency dependent circle such that its radius to the ear approximates  $\frac{\lambda}{4}$ . This reduces the cross talk to the contralateral ear.

For the beam depicted in 2.21, not only the position of the focus is set frequency dependent, but also the number of considered focus points that build the focus circle. Low frequencies (that have a larger wavelengths) are weighted with more focus points.



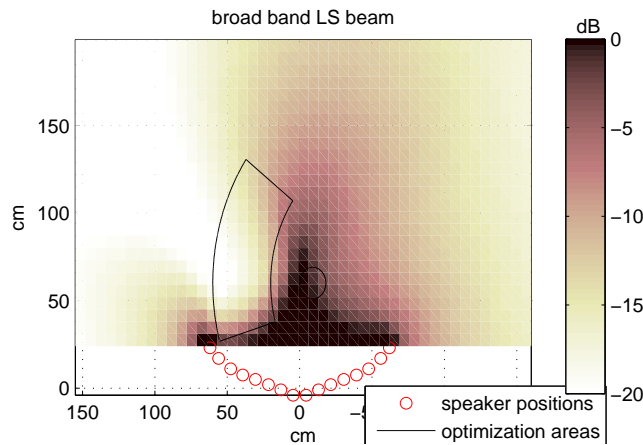


**Figure 2.21:** Broad-band (300-2500 Hz) sound pressure distribution of LSB with a frequency dependent focus area. For this illustration the focus area (i.e. the circle) of a middle wavelength was drawn into the pressure distribution. The sound pressure in the shaped area is desired to be zero, again.

A more detailed analysis of the LSBs will follow in section 2.7, but it can already be anticipated that the inversion of matrix  $(\mathbf{G}^H \mathbf{G})$  can cause trouble. If the ratio between the smallest and the largest singular value of  $(\mathbf{G}^H \mathbf{G})$  (i.e. the condition number) becomes too large, two problems might occur:

1. Numerical round-off errors.
2. Small variations of the matrix elements (e.g. differences between the idealized and the real transfer functions) lead to large aberrations after inversion.

Smaller condition numbers can be gained if the inverse matrix is regularized with the singular value decomposition (SVD). The SVD decomposes a  $n \times m$  matrix  $M$  into

$$\mathbf{M} = \mathbf{U} \mathbf{\Sigma} \mathbf{V}^H, \quad (2.28)$$

where  $\mathbf{U}$  is a  $n \times n$  and  $\mathbf{V}$  a  $m \times m$  unitary matrix.  $\mathbf{\Sigma}$  is a diagonal matrix with the size of  $\mathbf{M}$  which contains the singular values of  $\mathbf{M}$  in decreasing order on its diagonal. The above mentioned errors can be reduced if small singular values are neglected. A commonly used criterion for the threshold of this regularization is derived from the energy of the singular values. Only the largest  $l$  singular values that reach a threshold of  $th$  percent of the total energy are considered. Once the matrix is decomposed as in eq.2.28, the regularized inverse can easily be obtained by taking the  $l$  first rows and columns of  $\mathbf{U}$ ,  $\mathbf{\Sigma}$  and  $\mathbf{V}$ .

$$\mathbf{M}_l^{-1} = \mathbf{V}_l \mathbf{\Sigma}_l^{-1} \mathbf{U}_l^H. \quad (2.29)$$

For the following LSB simulations with SVD, a threshold of 99% has been chosen.

The next section, however, introduces a beamforming method that works without matrix inversion.

## 2.5 Maximum Energy Difference Beamforming

The Maximum Energy Difference beamformer (MEDB) introduced by Shin et al. [2009] tries to maximize the difference between the sound energy in the focus point and the average sound energy in the other control points. Shin et al. [2009] define the sound energy  $E(\omega)$  as

$$E(\omega) = p(\omega)^* p(\omega). \quad (2.30)$$

In the focus point  $E$  can be predicted by

$$\begin{aligned} E_{\text{focus}} &= (\mathbf{h}^T \mathbf{q})^* \mathbf{h}^T \mathbf{q} \\ &= \mathbf{q}^H \mathbf{h}^* \mathbf{h}^T \mathbf{q}. \end{aligned} \quad (2.31)$$

The average sound intensities of the other  $N$  control points can be rewritten in the same way

$$E = \frac{1}{N} \mathbf{q}^H \mathbf{G}^H \mathbf{G} \mathbf{q}. \quad (2.32)$$

The difference of sound intensities yields

$$\begin{aligned} E_{\text{focus}} - E &= \mathbf{q}^H \mathbf{h}^* \mathbf{h}^T \mathbf{q} - \mathbf{q}^H \mathbf{G}^H \mathbf{G} \mathbf{q} \\ &= \mathbf{q}^H (\mathbf{h}^* \mathbf{h}^T - \mathbf{G}^H \mathbf{G}) \mathbf{q}. \end{aligned} \quad (2.33)$$

To obtain a meaningful cost function, this difference requires another constraint. It is set into relation with the power of the source strength vector, which is proportional to  $\mathbf{q}^H \mathbf{q}$ . We get

$$J(\mathbf{q}) = \frac{\mathbf{q}^H (\mathbf{h}^* \mathbf{h}^T - \alpha \mathbf{G}^H \mathbf{G}) \mathbf{q}}{\mathbf{q}^H \mathbf{q}}, \quad (2.34)$$

wherein  $\alpha$  is a tuning factor, that allows to put more or less weight on the sound energy at the focus point alone. If  $\alpha = 0$ , the cost function relates the energy at the focus point with the power of the source strength vector. In microphone array literature, like e.g. in Brandstein and Ward [2001] this relation is known as white noise gain (WNG)

$$\text{WNG}(\omega) = 10 \log \left( \frac{|\mathbf{h}^T \mathbf{q}|^2}{\mathbf{q}^H \mathbf{q}} \right). \quad (2.35)$$

For microphone arrays, the WNG compares the amplification of the focus point with the amplification of spatially uncorrelated noise. For loudspeaker arrays, it compares the input power

with the outcome at the focus point, but is still referred to as white noise gain here.

Before equation (2.34) will be differentiated, it has to be rearranged to

$$\mathbf{q}^H \mathbf{q} J(\mathbf{q}) = \mathbf{q}^H (\mathbf{h}^* \mathbf{h}^T - \alpha \mathbf{G}^H \mathbf{G}) \mathbf{q}. \quad (2.36)$$

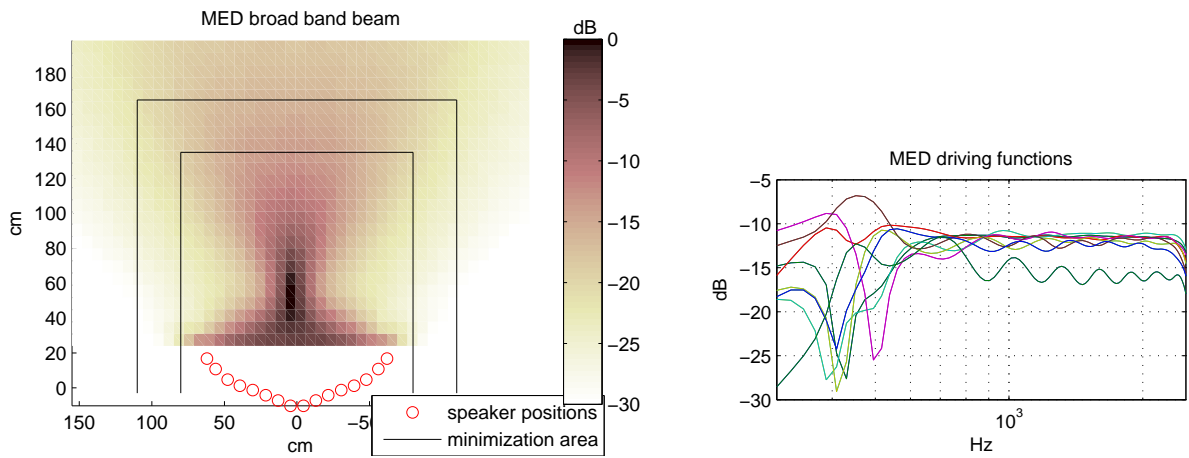
The differentiation of  $J$  with respect to  $\mathbf{q}$  is

$$2\mathbf{q} J(\mathbf{q}) + \mathbf{q}^H \mathbf{q} J(\mathbf{q}) \frac{d}{d\mathbf{q}} = 2 (\mathbf{h}^* \mathbf{h}^T - \alpha \mathbf{G}^H \mathbf{G}) \mathbf{q}. \quad (2.37)$$

$J(\mathbf{q})$  has a maximum where  $J(\mathbf{q}) \frac{d}{d\mathbf{q}} = 0$ . It follows that

$$\mathbf{q} J(\mathbf{q}_{\text{opt}}) = (\mathbf{h}^* \mathbf{h}^T - \alpha \mathbf{G}^H \mathbf{G}) \mathbf{q}. \quad (2.38)$$

This is a eigenvalue problem, and  $\mathbf{q}_{\text{opt}}$  is the eigenvector that corresponds to the highest eigenvalue  $J(\mathbf{q}_{\text{opt}})$ . The MEDB is thus a beamforming algorithm that can be solved without matrix inversion. The MEDB that tries to maximize the sound intensity difference between the focus point and the already known minimization area is depicted in Fig.2.22. A value of  $\alpha = 36$  brings a trade off between the WDSB and the LSB.



- (a)** Broad band (300-2500 Hz) pressure distribution of a MEDB. The sound energy difference between the focus point and the frame around the arrangement is maximized.
- (b)** The MED driving functions for the given control points and a tuning factor  $\alpha = 36$  have notch filters at low frequencies in order to reach a narrow beam width.

**Figure 2.22:** Pressure distribution and control point disposition of a MEDB with corresponding driving functions.

## 2.6 Minimum Variance Distortionless Response Beamforming

The LSB and the MEDB are both optimization methods that have to be applied to several frequency bins. Still, they do not have a constraint of producing a flat frequency response in the focus point. (See also Sec.2.7). The Minimum Variance Distortionless Response beamformer (MVDR) minimizes the sound intensity in the control points (eq.(2.32)) and enforces the source strength vector to sound pressure at unity gain at the focus point. Its constraint is

$$1 = \mathbf{h}^T \mathbf{q} = \mathbf{q}^H \mathbf{h}^*. \quad (2.39)$$

The optimization problem can be solved with the Lagrange multiplier  $\lambda$ . The Lagrange function  $J(\mathbf{q})$  consists of the function that has to be minimized plus the constraint function, multiplied with  $\lambda$

$$J(\mathbf{q}) = \mathbf{q}^H \mathbf{G}^H \mathbf{G} \mathbf{q} + \lambda (\mathbf{h}^T \mathbf{q} - 1). \quad (2.40)$$

Its derivative with respect to  $\mathbf{q}$  is set to zero

$$0 \stackrel{!}{=} 2\mathbf{q}^H \mathbf{G}^H \mathbf{G} + \lambda \mathbf{h}^T, \quad (2.41)$$

and delivers  $\mathbf{q}_{\text{opt}}$ , the location of the minimum of the Lagrange function

$$\mathbf{q}_{\text{opt}}^H = -\frac{\lambda}{2} \mathbf{h}^T (\mathbf{G}^H \mathbf{G})^{-1}. \quad (2.42)$$

Inserting this solution into equation (2.39)

$$1 = -\frac{\lambda}{2} \mathbf{h}^T (\mathbf{G}^H \mathbf{G})^{-1} \mathbf{h}^*, \quad (2.43)$$

yields  $-\frac{\lambda}{2}$ . Hence, the optimal solution for  $\mathbf{q}$  is

$$\mathbf{q}_{\text{opt}}^H = \frac{\mathbf{h}^T (\mathbf{G}^H \mathbf{G})^{-1}}{\mathbf{h}^T (\mathbf{G}^H \mathbf{G})^{-1} \mathbf{h}^*}. \quad (2.44)$$

A broad band MVDR beam for the given minimization area is depicted in Fig.2.23. Like for the LSB, matrix inversion is required to get a solution for  $\mathbf{q}_{\text{opt}}$ . The influence of SVD regularization on the MVDR beam is investigated in the following section. Yet other possibilities for LS- and MVDR constraints can be found in Guldenschuh and Sontacchi [2009].

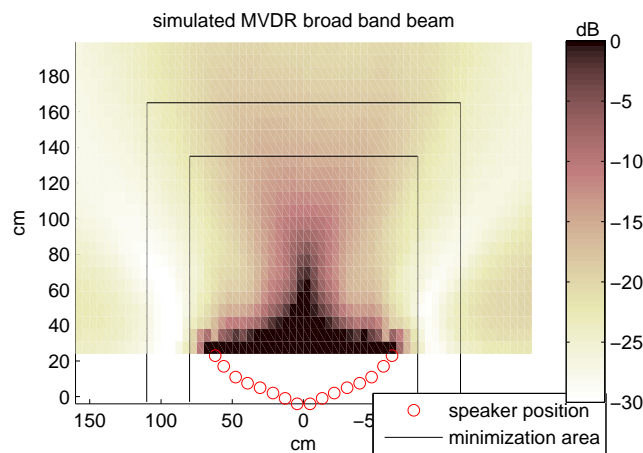


**Figure 2.23:** Broad band (300-2500 Hz) pressure distribution of a MVDRB. The pressure in the control points should be minimized, except for the focus point in the center, which is constrained to yield a constant gain for all frequencies.

## 2.7 Comparison of the Introduced Beamforming Methods

The four introduced beamforming methods will be compared in terms of their:

- Sound pressure attenuation
- SRR
- Frequency response in the focus point
- WNG
- Filter length and,
- Condition number in case of matrix inversion

The last four points are explicitly discussed in section 2.7.1 to 2.7.4 and section 2.7.5 gives an overall comparison of the beamforming performances. A central focusing position is chosen as reference for the comparison. The problems and benefits of the different beamforming methods can be well illustrated for this reference. The minimization areas of the different methods are depicted in the previous sections. Only the LSB was applied to two different optimization constraints. In the following the LSB with the minimization frame, (as depicted in Fig:2.19) is simply referred to as LSB, while the LSB with the frequency dependent focusing area is explicitly mentioned as  $LSB_{\text{freq.dep.}}$ . The influence of the SVD regularization is only shown for the MVDRB and the LSB. All figures and data of the  $LSB_{\text{freq.dep.}}$  have been derived with SVD, too.

### 2.7.1 Condition Number

The condition numbers of  $(\tilde{\mathbf{G}}^H \tilde{\mathbf{G}})$  and  $(\mathbf{G}^H \mathbf{G})$  (i.e. for LS- and the MVDR beam, respectively) are very similar and differ by less than 1 dB. In particular, condition is very poor for low frequencies. The improved condition numbers after regularization using SVD are depicted in Fig.2.24. The condition number is reduced to 25 dB. This prevents round-off errors and

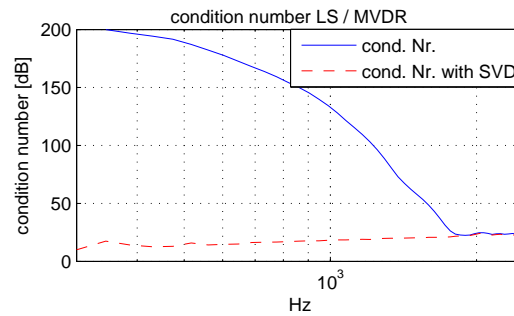
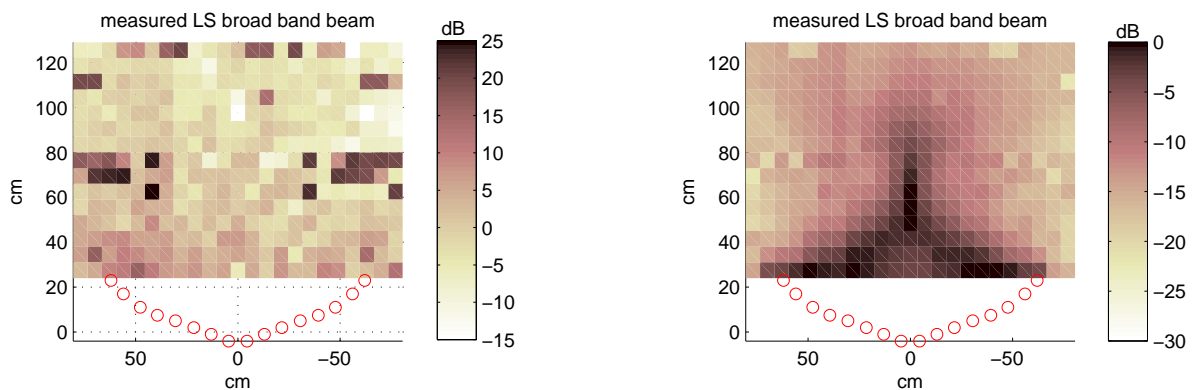


**Figure 2.24:** The condition numbers of  $(\tilde{\mathbf{G}}^H \tilde{\mathbf{G}})$  and  $(\mathbf{G}^H \mathbf{G})$  (of the LSB and the MVDRB, respectively) are nearly identical. This is why only one curve has been drawn for both. They have very low singular values at low frequencies, which are neglected by the SVD regularization.

yields robustness against mismatches in the array geometry and the loudspeaker characteristics. Fig.2.25 undermines the gain of robustness. The LS driving functions that have been derived over the (ideal) free field Green's functions are applied to the measured transfer functions. The result is a completely deteriorated sound field, because the measured transfer functions differ from the idealized ones. The specific influence of phase and amplitude differences as well as loudspeaker displacements have been investigated by Mabande and Kellermann [2007]. The beam is rendered correctly, if the driving functions are regularized.



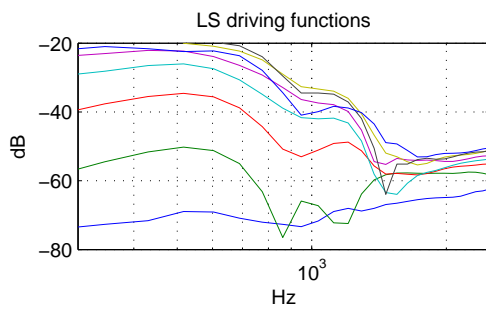
**(a)** Without SVD the LSB causes a undesired random sound field if the real life conditions are not exactly the same as for the simulation.

**(b)** The LSB with SVD regularization also works fine for imperfect hardware and mismatches in the array geometry.

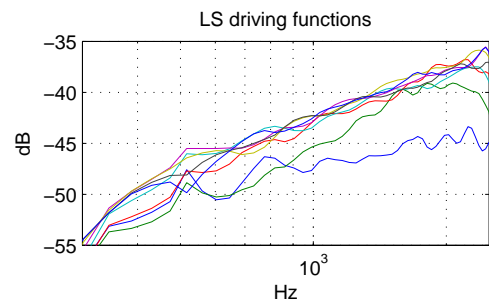
**Figure 2.25:** The LS driving functions were applied to the measured transfer functions. The aberrations of the measurement data from the ideal transfer functions cause a waste sound field, if no SVD is applied. The MVDRB delivers equal results.

## 2.7.2 Driving Functions

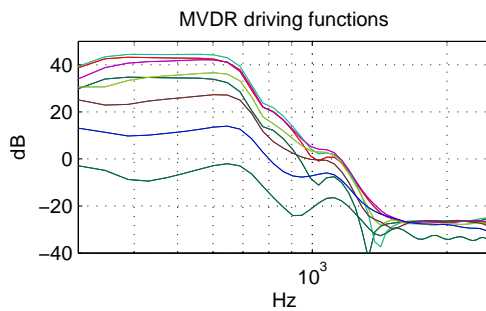
The changes of the spectrum of the driving functions due to the SVD regularization can be seen in Fig.2.26. The excessive bass boost is suppressed. For the implementation of a beamformer however, it is more important to know the temporal behavior of the filters. Impulse-responses examples of the driving functions for the superdirective beamformers are shown in Fig.2.27. The LS- and the MVDR driving functions decay smoothly and do not have a lot of pre-pulses, while the  $LS_{\text{freq.dep}}$ - and MED driving functions have strong ripples before and after the impulse. In order to get a comparable value for the required length of the filters, the number of samples that have got 98 % of the impulse-response energy are considered as filter length. 1 % of the total energy lies before and after the considered samples, respectively. The comparison of the filter lengths follows in table 2.1.



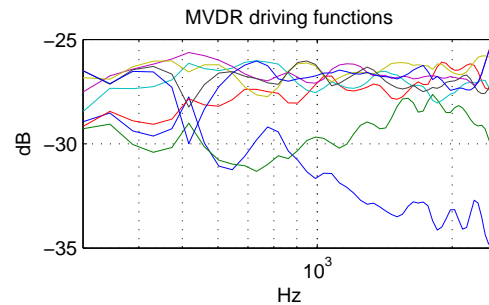
**(a)** LSB without SVD. The dynamic of  $q$  is very high. Low frequencies are strongly amplified.



**(b)** LSB with SVD. The basses are strongly reduced.



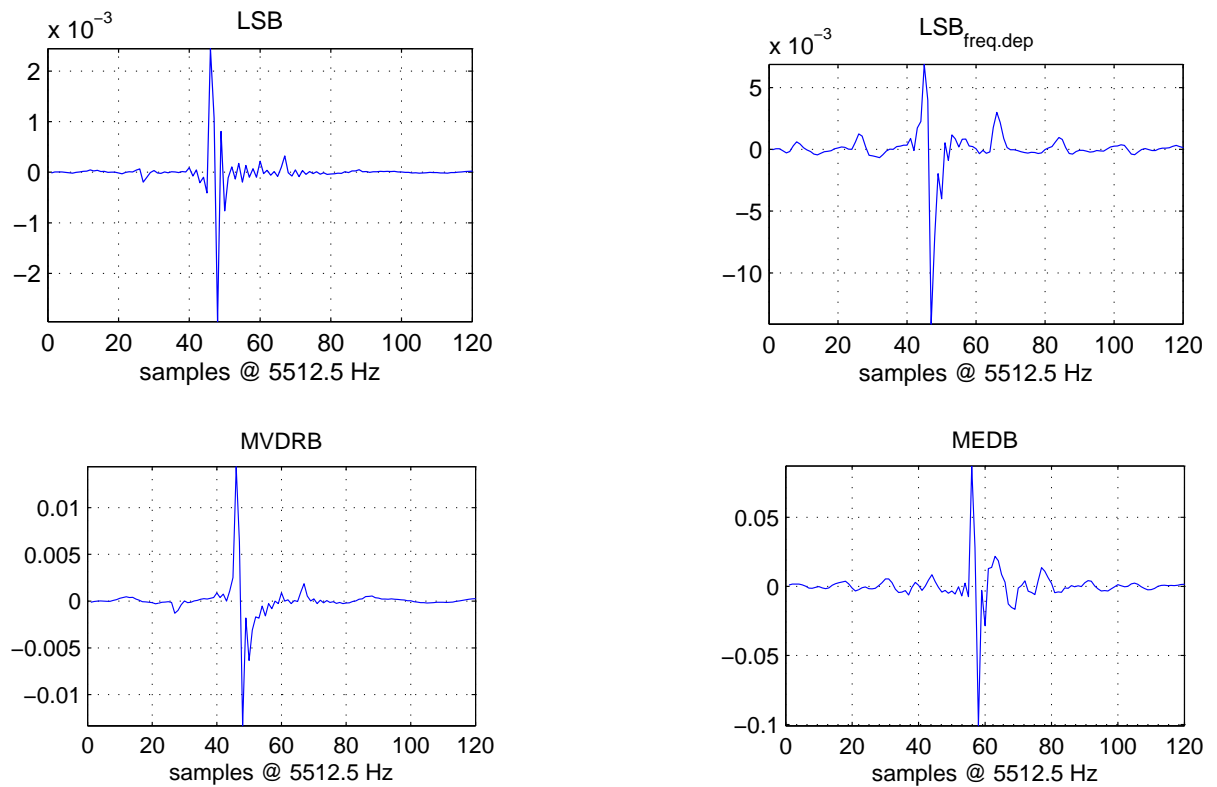
**(c)** MVDRB without SVD. Low frequencies are strongly amplified, even more than in the case of the LSB.



**(d)** MVDRB with SVD. The SVD causes quite flat spectrums for the MVDR driving functions.

**Figure 2.26:** Frequency response of the LS- and MVDR driving function. Only the first 8 frequency responses are shown. They equal the last 8, for the focus point is in a central position.





(c) The LS- and MVDR driving functions have a fast decay of the impulse response.

(d) The  $LS_{\text{freq.dep}}$ - and MED driving functions have strong ripples before and after the impulse.

**Figure 2.27:** Example of driving functions for the superdirective beamformers in the time domain.

### 2.7.3 White Noise Gain

The WNG relates the SPL at the focus point to the energy of the loudspeaker signals and is therefore a measure of the beamformer's efficiency. Firstly, the influence of the SVD regularization is investigated again. The LS- and MVDR beams produce a low sound pressure in the horizontal minimization area, but radiate extensively into every other direction if no regularization is applied. Fig.2.28 shows the 3D directivity of an MVDR beam the improvement due to SVD regularization.

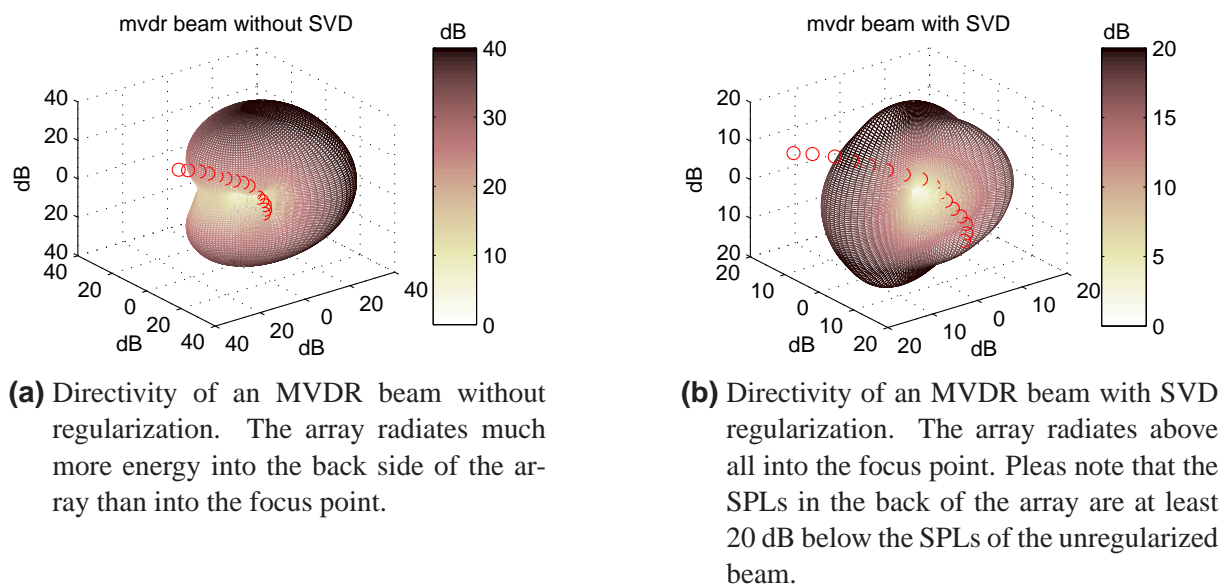
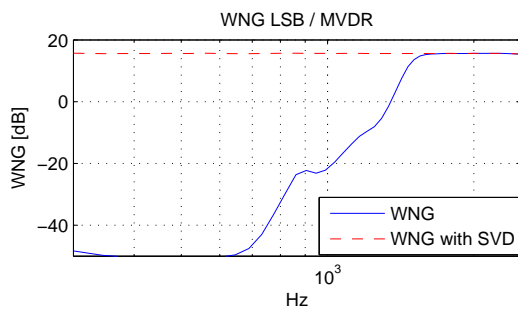
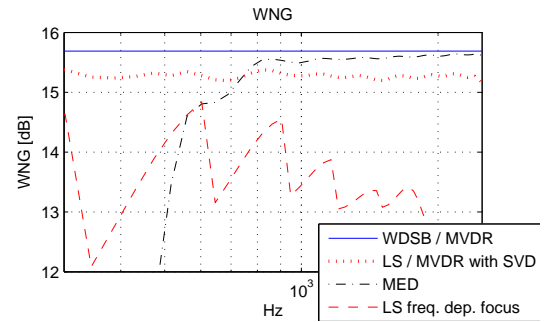


**Figure 2.28:** 3D directivity of a MVDR beam. Without regularization, the acoustical power of the MVDR beam is about 20dB higher. Still it is impressive, how the sound pressure in the minimization area is suppressed.

Fig.2.29a shows the improvement of the WNG due to the regularization. At low frequencies it is increased by almost 70 dB. This makes the LS- and the MVDR beam almost as efficient as the Weighted Delay & Sum beam that has the best possible WNG (as in Brandstein and Ward [2001]). The comparison between the WNGs of the different beamformers can be seen in Fig.2.29b. The MED beamformer and the  $LSB_{\text{freq.dep.}}$  have the worst WNG.



(a) The white noise gain of the LS and MVDR beam are almost identical, again. Thus, both are represented by one line. SVD regularization improves the WNG, especially for low frequencies.

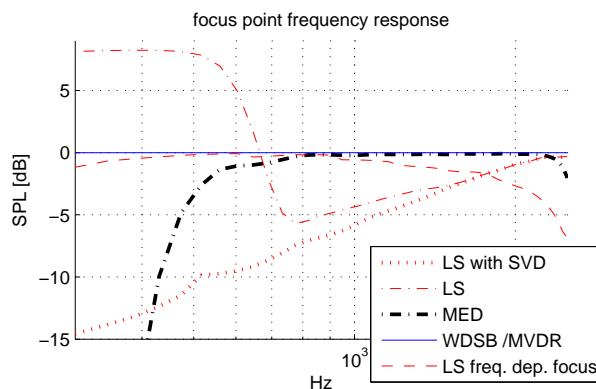


(b) The Weighted Delay & Sum beam has an optimal WNG. It requires the least input energy to derive the demanded SPL at the focus point. The regularized LS- and MVDR beam show almost the same performance, while the MED beam decreases to -15 dB for low frequencies.

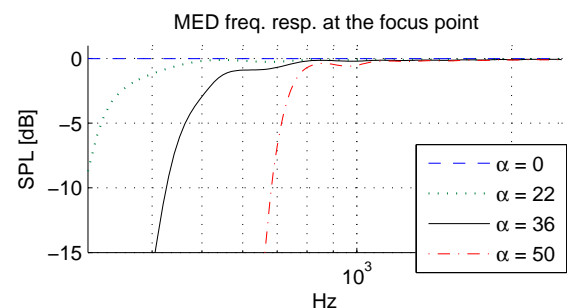
Figure 2.29

### 2.7.4 Frequency Response at the Focus Point

The WNG and the frequency response of the driving functions determine the frequency response in the focus point. This can be clearly observed for the regularized LSB. The gain of its driving functions (Fig.2.26b) raises with the frequency, but the WNG is flat. As a consequence, the frequency response in the focus point raises with the frequency, too. The frequency responses of all beamformers are depicted in Fig.2.30a. It is remarkable that the  $LSB_{freq.dep.}$  produces a



(a) All beamforming methods, except for the LSB and the MEDB cause a flat frequency response in the focus point. It is remarkable that the LSB with frequency dependent focusing area causes a quite flat spectrum, too.



(b) MED frequency response at the focus point. The high pass cut-off frequency increases with the tuning factors  $\alpha$ .

Figure 2.30

quite flat spectrum at the focus point. In contrast to the LSB, the  $LSB_{freq.dep.}$  does not attenuate the basses. This is because more focus points are considered for low frequencies (as explained

in Fig.2.20). Therefore, the  $LSB_{freq.dep.}$  puts more effort into reaching the unity gain at low frequencies.

The frequency response yielded by the MED beam depends on the tuning factor  $\alpha$ . In general, it has a high pass characteristic. Fig.2.30b shows that higher values of  $\alpha$  cause higher cut-off frequencies. A tuning factor of  $\alpha = 0$  optimizes the WNG and hence yields the same result as the Weighted Delay & Sum beamformer.

## 2.7.5 Overall Comparison

Table 2.1 gives an overview of the comparison. The LSB and the MVDR are only considered with regularization for the beams are not applicable otherwise, as it has been shown previously. Apart from the average WNG and the filter length, the SRR as defined in section 2.3.2 is stated. Except for the  $LSB_{freq.dep.}$ , all optimization methods aimed to produce a low sound pressure in a frame around the user space.  $SPL_{frame}$  denotes the average sound pressure level in this frame. The  $LSB_{freq.dep.}$  was introduced to produce a low SPL in an interaural distance of the focus point. A point 20 cm next to the focus point in parallel to the x axis was chosen as reference for  $SPL_{20cm}$ . This reference point is also depicted in Fig.2.31. The  $SPL_{frame}$  and the  $SPL_{20cm}$  give

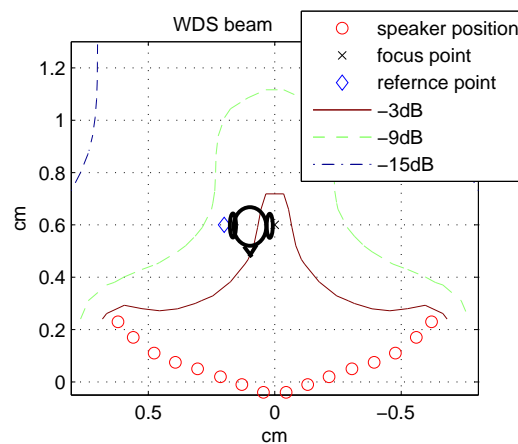


**Figure 2.31:** Reference point for  $SPL_{20cm}$ . If the beam is steered to the ear of a user, this point is meant to mark the position of the contralateral ear.

good reference values about the sound pressure decay. The pressure decay of the beamformers in 3 bands are shown in appendix B. As last measure, the variations of the frequency response in the focus point is introduced. It is the standard deviation  $\sigma$  of the SPL in dB over frequency.

The table shows that the LS- and the MED beams have low average SPLs in the minimization areas and a good SRR. However the simple Weighted Delay & Sum beam has comparable results and the advantage that it causes a flat frequency response in the focus point. Besides, it can easily be realized with a delay line and one multiplication only. Its sound pressure in the focus point is 18 dB higher than the SPL of a reverberant room. In Moore [1995], this difference is stated to be below the masking level. Thus, it can be assumed that coworkers in the

same room are not disturbed by the loudspeaker signals. The  $\text{LSB}_{\text{freq.dep.}}$  and the MVDR do not really perform better than the WDSB, but are more complex in their realization. Finally, it can be concluded that the WDSB is the most feasible beamformer for a dynamic application, like it is outlined in the introduction. Its realization is very processing efficient and its results are very satisfying. Consequently the WDSB is used for further investigations on transaural stereo with focused sound. These investigations follow in the next chapter.

**Table 2.1:** Comparison of the beamforming methods. The LSB and the MED have very good results for the SPL decay and the SRR, however they have a strong variations of the frequency response in the focus point. The MVDRB and the  $\text{LSB}_{\text{freq.dep.}}$  do not really perform better than the WDSB. Considering its efficient implementation, the WDSB is the most feasible beamforming method for the given conditions.

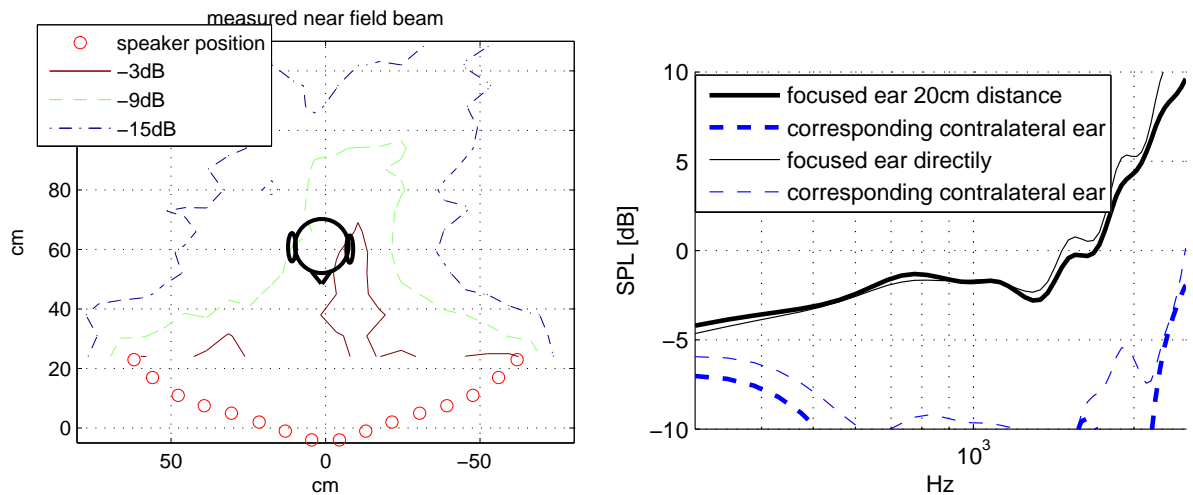
	WDSB	MVDR	$\text{LSB}_{\text{freq.dep.}}$	MED	LSB
filter length	delay line + multiplication	39	69	99	20
average WNG	15.7 dB	15.5 dB	13.4 dB	10 dB	15.5 dB
SRR	17.5 dB	17.5 dB	15.7 dB	18 dB	19 dB
$\text{SPL}_{\text{frame}}$	-17.5 dB	-18 dB	-13 dB	-19 dB	-20 dB
$\text{SPL}_{20\text{cm}}$	-11 dB	-11 dB	-13 dB	-14 dB	-15 dB
$\sigma$	0 dB	0 dB	1.5 dB	6 dB	4 dB

# Chapter 3

## Transaural Stereo

### 3.1 Concept of Transaural Stereo for a Loudspeaker Array

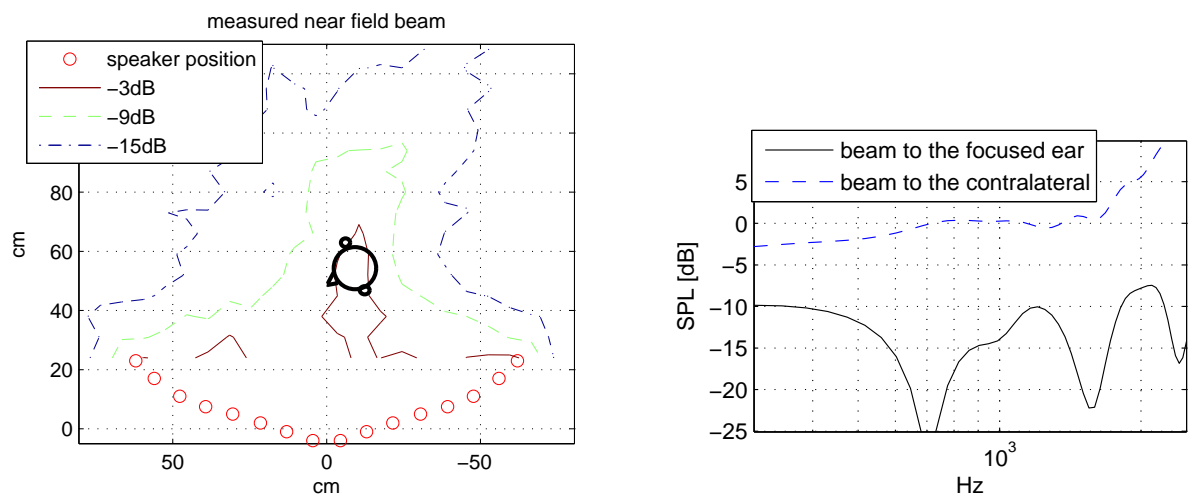
The beamformers (described in the previous chapter) minimize the total energy that excites the sound field. They also cause a natural channel separation (between the left ear signal and the right ear signal), if the beams are steered to the ears of the user. As stated in the introduction, this channel separation is important for a transaural stereo application. In Fig.3.1a shows the SPL contours of a measured WDSB. The head symbol marks the listener position. The broad band pressure at the position of the contralateral ear is already attenuated by 9 dB. The channel separation over frequency was measured with a dummy head. Fig.3.1b shows the channel separation of a beam to the eardrum and a beam with a focus 20 cm outside of the ear. Low frequencies have a larger beam width and, therefore, causes a higher cross talk. The beam, focused 20 cm outside of the ear, causes less cross talk for low frequencies, with hardly any loss of channel separation for high frequencies.



(a) The broad band sound pressure decay at the position of the contralateral ear is -9 dB. (b) SPL of the crosstalk over frequency. The beam width decreases with the frequency. Therefore the crosstalk decreases, too. The channel separation of low frequencies is 1 dB better, if the beam is focused 20 cm away from the ear.

**Figure 3.1:** Channel separation due to a WDS beam that is steered to one ear.

If the ear is turned away from the array, the results are deteriorate. This particular constellation is depicted in Fig.3.2 and the corresponding cross talk over frequency in Fig.3.2b. Anyway,



(a) No channel separation due to beamforming can be assumed if the contralateral ear is facing the loudspeaker array. (b) The cross talk is even higher than the beam at the rear focused ear itself.

**Figure 3.2:** There is no channel separation, if the focused ear is turned away from the loudspeaker array.

for either case a cross talk canceler (XTC) has to be applied, for two reasons:

1. To reduce the cross talk (above all, for the low frequencies).

2. To equalize the frequency response at the focused ear.

The second point is not really included in the term cross talk canceler, but it is equally important for a transaural stereo applications. The binaural signals have to reach the ears without alteration. Therefore the XTC has to cause a flat frequency response at the entrance to the ear channel.

The relation between the binaural input signals  $L$  and  $R$  and the signals at the eardrum  $E_l$  and  $E_r$  is given in eq.(3.1). All variables express quantities in the frequency domain. The dependency on  $\omega$ , however, is omitted for the sake of compactness.  $L$  and  $R$  are split into  $2 \times 16$  loudspeaker signals in the beamforming stage ( $q_{ji}$ ). These  $2 \times 16$  loudspeakers signals reach

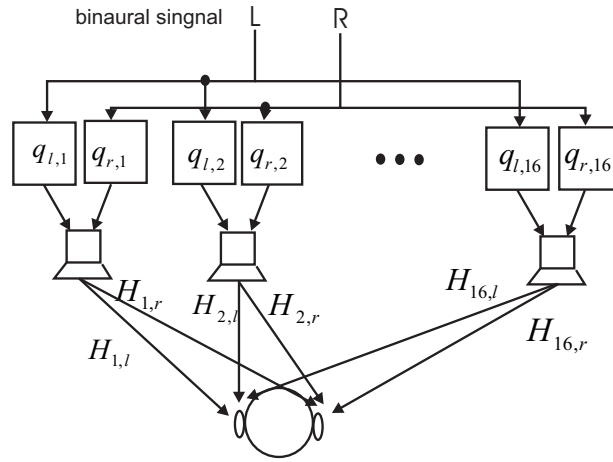


**Figure 3.3:** The binaural signals are delayed and weighted by the complex factors  $q_{i,j}$  and reach the ears via the HRTFs  $H_{j,i}$ . The overall transfer functions are derived by superimposing these weighted HRTFs.

the ears over  $16 \times 2$  head related transfer functions  $H_{ij}$

$$\begin{pmatrix} E_l \\ E_r \end{pmatrix} = \begin{pmatrix} H_{1,l} & H_{2,l} & \cdots & H_{16,l} \\ H_{1,r} & H_{2,r} & \cdots & H_{16,r} \end{pmatrix} \begin{pmatrix} q_{l,1} & q_{r,1} \\ q_{l,2} & q_{r,2} \\ \vdots & \vdots \\ q_{l,16} & q_{r,16} \end{pmatrix} \begin{pmatrix} L \\ R \end{pmatrix}. \quad (3.1)$$

These transfer paths are also schematized in Fig.3.3. With the definition of a composite transfer matrix

$$\mathbf{T} = \begin{pmatrix} T_{ll} & T_{rl} \\ T_{lr} & T_{rr} \end{pmatrix} = \begin{pmatrix} H_{1,l} & H_{2,l} & \cdots & H_{16,l} \\ H_{1,r} & H_{2,r} & \cdots & H_{16,r} \end{pmatrix} \begin{pmatrix} q_{l,1} & q_{r,1} \\ q_{l,2} & q_{r,2} \\ \vdots & \vdots \\ q_{l,16} & q_{r,16} \end{pmatrix}, \quad (3.2)$$

equation (3.1) simplifies to

$$\begin{pmatrix} E_l \\ E_r \end{pmatrix} = \mathbf{T} \begin{pmatrix} L \\ R \end{pmatrix}. \quad (3.3)$$



The XTC matrix  $\mathbf{C}$  is applied to the input signals  $L$  and  $R$

$$\begin{pmatrix} \hat{E}_l \\ \hat{E}_r \end{pmatrix} = \mathbf{T}\mathbf{C} \begin{pmatrix} L \\ R \end{pmatrix}, \quad (3.4)$$

in order to achieve the desired ideal transmission

$$\mathbf{T}\mathbf{C} = \mathbf{I}, \quad (3.5)$$

where  $\mathbf{I}$  is the identity matrix. Thus,

$$\mathbf{C} = \mathbf{T}^{-1}. \quad (3.6)$$

The calculation of the XTC matrix bears 2 problems:

1. The transfer matrix  $\mathbf{T}$  has to be identified.
2. This transfer function matrix has to be inverted.

**ad 1.**

The transfer matrix is derived over the multiplication of the beamforming weights with the head related transfer functions (HRTFs) from all loudspeakers to the left and right ear, respectively. The beamforming weights can be calculated with knowledge about the position of the user and the loudspeaker array, as it is deduced in chapter 2. The HRTFs are derived from a data base. For the following simulations and measurements, a data base of 36 HRTFs in the horizontal plane has been used. The HRTFs have been measured with a dummy head in  $10^\circ$  steps. Positions between the measured grid are linearly interpolated in phase and amplitude. To take different distances into account, suitable delays and gains are applied on the interpolated HRTFs.

**ad 2.**

Like mentioned in section 2.4, matrix inversion is problematic if the determinant  $\det(\mathbf{T})$  is close to zero. This can be prevented if a bias  $\beta$  is added to the determinant. This regularization may be frequency dependent like it is shown in Kirkeby and Nelson [1999]. The inverted determinant becomes

$$\det(\mathbf{T})^{-1} = \frac{\det(\mathbf{T})^H}{\|\det(\mathbf{T})\|^2 + \beta \|H\|^2}, \quad (3.7)$$

wherein  $H$  is a filter that determines the frequencies on which  $\beta$  works. The absolute values of  $\det(\mathbf{T})$  have been investigated for 384 head positions with  $0^\circ$  and  $30^\circ$  head rotation each. The head positions correspond to the measurement points of Fig.2.7a. The lowest values of the determinant always appeared at 300 Hz where the cross talk path is equally strong as the direct path. Still, the determinant does not fall under an absolute value of 0.09, which of course is no numerical problem for inversion. Still, the determinant can lead to dynamical problems if the

ratio between the highest and the lowest value becomes to large. The beamformer, in general, makes sure that the direct paths ( $T_{ll}$  and  $T_{rr}$ ) have higher amplitudes than the off-diagonal elements. In the worst cases, (as depicted in Fig.3.2) the cross talk response can be equally loud as the direct paths. Therefore, the dynamic range of  $T_{ll}$  and  $T_{rr}$  need to be investigated only. Fig.3.4 shows the level lines within which a certain dynamic level is not exceeded. The

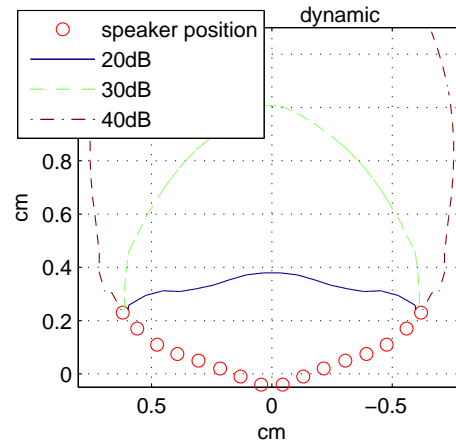


**Figure 3.4:** The dynamic range does not exceed 30 dB in the major part of the working area. This is a value that ordinary sound equipment should cope with.

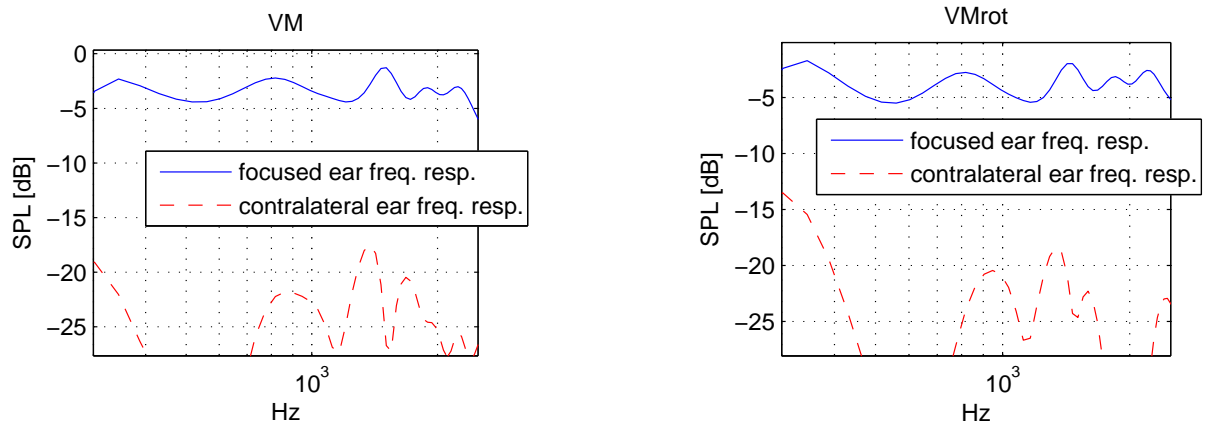
frequency response is bounded within a range of 40 dB across the whole working area. If the sound equipment cannot cope with this dynamic range, the regularization factor  $\beta$  needs to take values greater than zero. The smallest value of  $\det(\mathbf{T})$  was  $\sim \frac{1}{10}$ . Choosing, e.g., a  $\beta$  that is a factor of 10 higher ( $\beta = 1$ ), reduces the dynamic of the basses by 20 dB; of course with the cost of a high pass characteristic in the ear signal.

## 3.2 Cross Talk Cancellation Results

Concerning the transfer functions, three factors are important to render a correct binaural signal:

1. A flat frequency response at the focused ear.
2. A high channel separation.
3. A uniform group delay of the transmitted energy. The transfer function to the focused ear should not only have a flat frequency response, but also a pulse like temporal behavior.

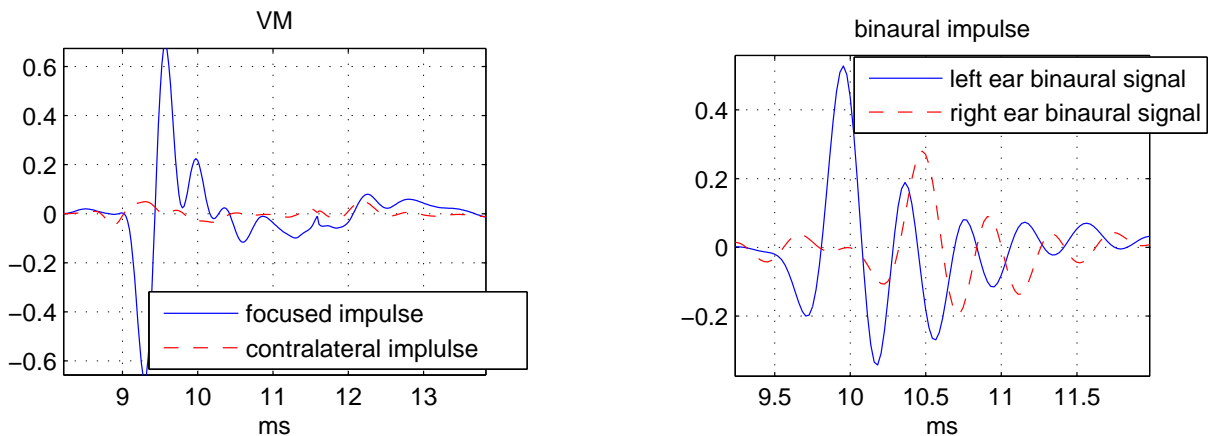
All following results are based on dummy head measurements. Fig.3.5 shows the improvement on the situations depicted in Fig.3.1 and 3.2, due to the cross talk canceler. The frequency response has a ripple of less than 5 dB and the channel separation is larger than 10 dB for all frequencies. For both cases, the temporal behavior (shown in Fig.3.6a) is pulse like and mainly



(a) Central position, the nose points to the array.

(b) Central position, 30° head rotation.

**Figure 3.5:** Frequency responses after XTC. Two effects can be observed: First, the channel separation is much higher, also for the low frequencies and second, the frequency response at the focused ear is equalized.



(a) For the focused ear, the temporal response of the XTC is a pulse. Its dispersion mainly comes due to the applied band pass filter. At the contralateral ear the impulse response is smeared out and compressed.

(b) A binaural impulse from the left (90°) was fed to the transaural beamformer for a central head position. There is a small pre-echo in the right ear binaural signal at 9.5 ms.

**Figure 3.6:** Temporal behavior of the XTC.

deteriorated by the band pass filter from 300 to 2500 Hz.

The frequency responses of the transaural beamformer were measured at 4 head positions with 0° and 30° rotation each. The positions are marked in Fig.3.7. The variations in the frequency responses are smaller than 6 dB and the channel separation is at least 10 dB for all positions. The amplitudes of all frequency responses are shown in Appendix C. The temporal behaviors equal the one presented in Fig.3.6. These results are satisfactory, however, they vary with the head position and rotation. A quality measure is introduced to assess the dependency

on these positions and rotations. As the temporal behavior looks equally good for all measurements, the quality measure  $Q$  only takes into account the channel separation and the ripple in the frequency response. The channel separation  $SPL_{\text{dif}}$  is simply given by the average amplitude difference in dB. The ripple  $SPL_{\text{var}}$  will be defined as the variance of the amplitude over frequency. The average channel separation is 14 dB in the worst case and 22 dB in the best case. The variance varies between 1 and 3 dB<sup>2</sup>. The two quantities are scaled to match their range and are added to

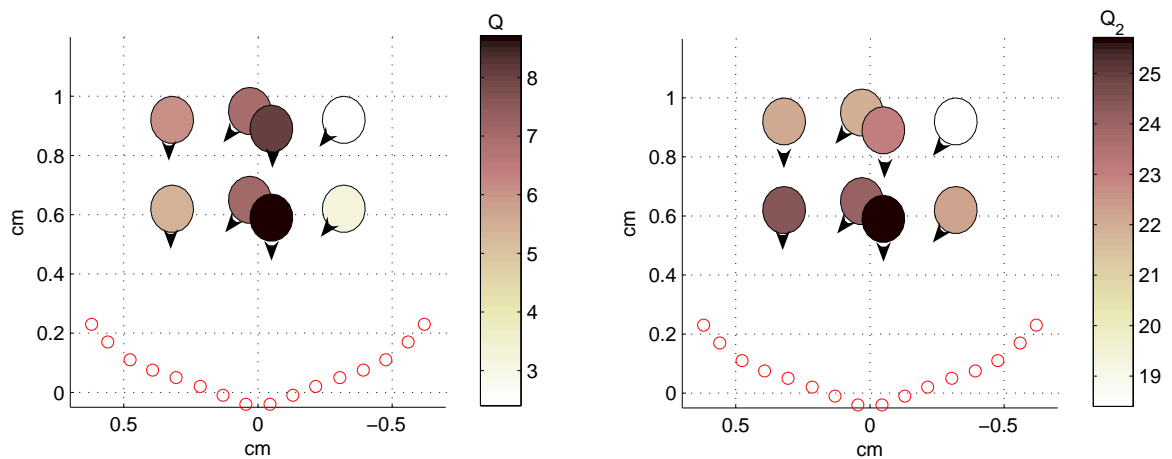
$$Q = \frac{1}{2}SPL_{\text{dif}} - 2 SPL_{\text{var}}. \quad (3.8)$$

Of course,  $SPL_{\text{var}}$  is desired to be small; as a consequence it is subtracted from  $SPL_{\text{dif}}$ . The results of  $Q$  can be seen in Fig.3.7a. The central positions have the best XTC conditions, while the side positions with 30°rotation have the worst.

Until now, only the correct binaural perception has been considered for the quality factor  $Q$ . The excitation of the room, however, should also be taken into account, as stated in the introduction. The SRR of the WDSB varies between 15 and 19 dB for the given head positions and has therefore the same range as the two already considered (scaled) properties. The quality measure  $Q_2$  includes the room excitation and is defined as

$$Q_2 = \frac{1}{2}SPL_{\text{dif}} - 2 SPL_{\text{var}} + SRR. \quad (3.9)$$

The results of  $Q_2$  are shown in Fig.3.7b. It can be concluded that the quality of the transaural beamformer decreases with the distance from the array, with the degree of head rotation and with the distance from the symmetry axis.



**(a)** XTC quality. Central positions and 0° head rotations have the best preconditions for a correct binaural perception.

**(b)** Transaural beamforming quality. The room excitation is included in the measure. Beams to the close side positions cause little room excitation (see also Fig.2.16b), that is why the close side head positions also perform better in terms of the transaural beamforming quality  $Q_2$ .

**Figure 3.7:** Evaluated head positions and rotations. Please note that the head positions on the symmetry axis are coincident for both rotations. They are only displaced for the representation. The quality of the transaural beamformer decreases with the distance from the array, with the degree of head rotation and with the distance from the symmetry axis.

# Chapter 4

## Resume and Outlook

### 4.1 Resume

Binaural signals evoke a spatial sound-impression if they are transmitted to the ears directly. They are used in various virtual- or augmented reality applications, in which they are mostly played back via headphones. Transaural stereo is a method that preprocesses binaural signals in order to play them back over loudspeaker in the room. The preprocessing is necessary because the transmission paths from the loudspeakers to the ears would cause a coloration of the binaural signals. Especially the cross talk from the left binaural signal to the right ear and vice versa leads to a grave alteration of the binaural signal which impairs the spatial impression.

In this thesis, a transaural stereo application with focused sound is introduced. The focusing bears two advantages. Firstly, it prevents a strong sound excitation of the room, and secondly, it achieves a better channel separation if the beams are steered to the ears. This is advantageous for cross talk cancellation because it already brings some channel separation, especially at high frequencies. A focused sound can be accomplished with an array of loudspeakers. The physical straightforward method of sound focusing is a Weighted Delay & Sum beamformer (WDSB). It delays the loudspeaker signals such that they coincide in a focus point, where they are added constructively. The geometrical properties (i.e. the loudspeaker positions and their distance to the focus point) suffice to calculate the delay times and the weights of the WDSB. It can easily be realized with a delay line and one multiplication per loudspeaker channel.

Superdirective beamformer like the Least Squares- (LS), the Maximum Energy Difference- (MED) and the Minimum Variance Distortionless Response (MVDR) beamformer have additional filters and are traditionally used to produce a smaller beam width (i.e an improved directivity). They use optimization algorithms to render the sound field for a given constraint. This constraint, however, does not necessarily have to be a small beam width. A low sound pressure in any point of a sound field can be forced. The LS and the MVDR algorithm require

matrix inversion. It turned out that the matrices that are to be inverted are ill conditioned for most constraints. Hence, regularization, using singular value decomposition (SVD) facilitate applicable LS and MVDR solutions. The MED algorithm leads to a eigenvalue problem which can be solved without matrix inversion. However, it demands filters that are five times as long as a LS- or MVDR filter to yield comparable results.

All mentioned beamforming methods were investigated in terms of their spatial pressure decay, their excitation of the room, their complexity and their frequency response at the focus point. Especially, they are compared with respect to their contribution to a effective cross talk cancellation. The LS- and the MED beamformer show very good results of directivity and sound pressure decay, but they do not produce a flat frequency response at the focus point. In contrast, the MVDR beamformer has the constraint of producing unity gain at the focus point. Also the LS beamformer can be tuned to produce an equalized spectrum at the focus point. However, they do not perform much better than the simple WDSB.

Finally, it can be concluded that the WDSB is the most feasible focusing method for the given constraints. Mainly it benefits from its low processing load and its optimal input / output relation. Subsequently, the WDSB has been applied to a loudspeaker array with 16 elements for which the cross talk cancellation matrix is deduced. Two kinds of measurements proof the concept and the functionality of the system. Firstly, the sound field has been measured with a microphone array in order to compare it with the simulated sound fields and second the cross talk canceler was evaluated with dummy-head measurements. A channel separation of at least 10 dB could be gained (even for head rotations which are difficult to handle) and the variations in the frequency response stay b 5 dB. low

## 4.2 Outlook

A prototype of the proposed transaural beamformer shall be evaluated at the Eurocontrol Experimental Center (EEC) in Brétigny-sur-Orge, France. The prospective evaluation concerns technical as well as psychological matters. The technical questions are: Does the transaural beamformer disturb neighboring air traffic controllers; and, in how far does it increase the noise level in the air traffic control center? The psychological aspects concern the concentration of air traffic controllers and its consequence on the error prevention. Commonly, air traffic controllers use stereo headphones whereas one channel is designated for the pilots of the air crafts and the other one for controllers of neighboring air space sectors. In contrast, the transaural beamformer produces spatialized sound, which makes the audio impression much more natural than this conventional stereo separation. In the evaluation, it should be investigated if the increase of comfort also leads to an increase of concentration and if the spatial separation of the communication partners can reduce communication mistakes.

Listening test at the Institute of Electronic Music and Acoustics will evaluate the perception of the transaural signals. In particular, it will be investigated if the virtual sound sources are located correctly and if their spatial distribution helps to distinguish between one from another.

Air traffic control communication suffers from a low bandwidth of 300 to 2500 Hz and additive transmission noise. The intelligibility of speech can be improved by artificial bandwidth extension like proposed in Schäfer [2008] as well as by multi band compression as in Domínguez [2009]. Both methods can easily be integrated into the system of the transaural beamformer. The transaural beamformer itself benefits from the low bandwidth, because it reduces the risk of spatial aliasing. It also has a positive influence on the cross talk canceler. The cross talk canceler is based on head related transfers functions (HRTFs). In general, these HRTFs are unique for every human as they depend on the geometry of ear, head and torso, too. The individuality of these geometries however has above all influence on higher frequencies. On the one hand, it can therefore be assumed, that the HRTFs, measured with the dummy head, will be good enough to provide accurate spatialized audio. On the other hand it raises the questions, if the HRTFs could not be modeled analytically. This would reduce the RAM allocation of the system, as the HRTF data base could be omitted. Finally, further beamforming methods can be investigated, like for example the MVDR beamformer with white noise gain constraint that was proposed by Mabande et al. [2009].



# Appendix A

## Notation

Throughout this thesis bold lowercase letters  $\mathbf{x}$  are meant to be vectors, bold uppercase letters  $\mathbf{X}$  matrices and italic letters  $x$  refer to scalar values.  $\mathbf{X}^T$  denotes matrix transposition,  $\mathbf{X}^H$  complex conjugate transposition and  $\mathbf{X}^*$  conjugation, only. In this thesis, the following physical symbols are used:

$j$		imaginary number $j = \sqrt{-1}$
$f$	[Hz]	frequency
$\omega$	[1/s]	radial frequency $\omega = 2\pi f$
$\lambda$	[m]	wave length
$c$	[m/s]	speed of sound
$k$	[1/m]	wavenumber $k = \frac{\omega}{c}$
$\nu$	[m/s]	sound particle velocity
$p$	[Pa]	sound pressure
$\rho$	[kg/m <sup>3</sup> ]	density
$P_{ac}$	[W]	acoustic power
$\vec{I}$	[W/m <sup>2</sup> ]	sound intensity

## Appendix B

# Comparison of the SPL Distribution of the Different Beamformers

The pressure decay of the beamformers are shown in 3 bands in Fig.B.1 to B.7. The cut off frequencies are logarithmically spaced to consider the sensitivity of the ear. It can be seen that the LSB and the MVDRB loose their steep decay towards the back end at low frequencies if SVD is applied. As it was shown in Fig.2.24, the SVD had the strongest impact on these low frequencies. It can be concluded that it is easier for the optimization methods to cause a narrow beam than a beam that has to decay towards the back end.

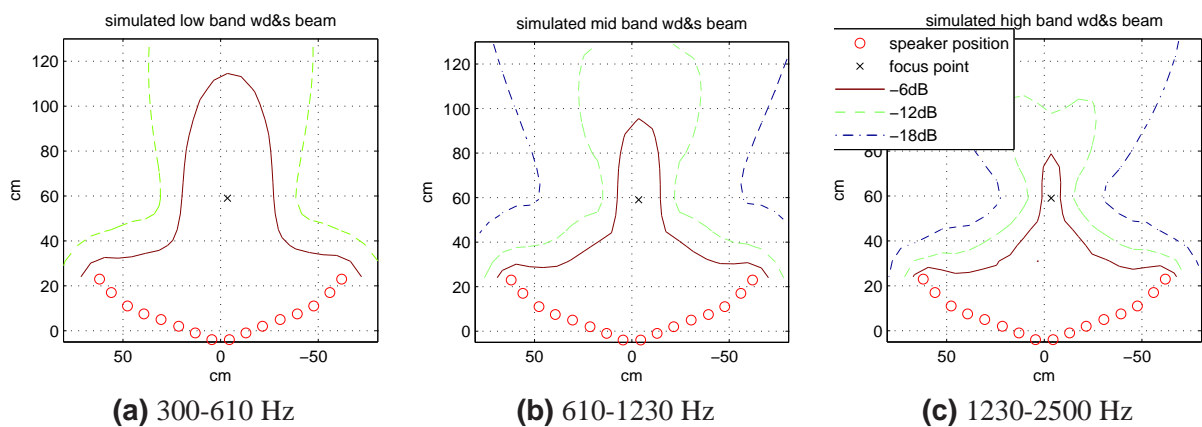


**Figure B.1:** Simulated WDSB in 3 bands. The beam width decreases with the frequency.

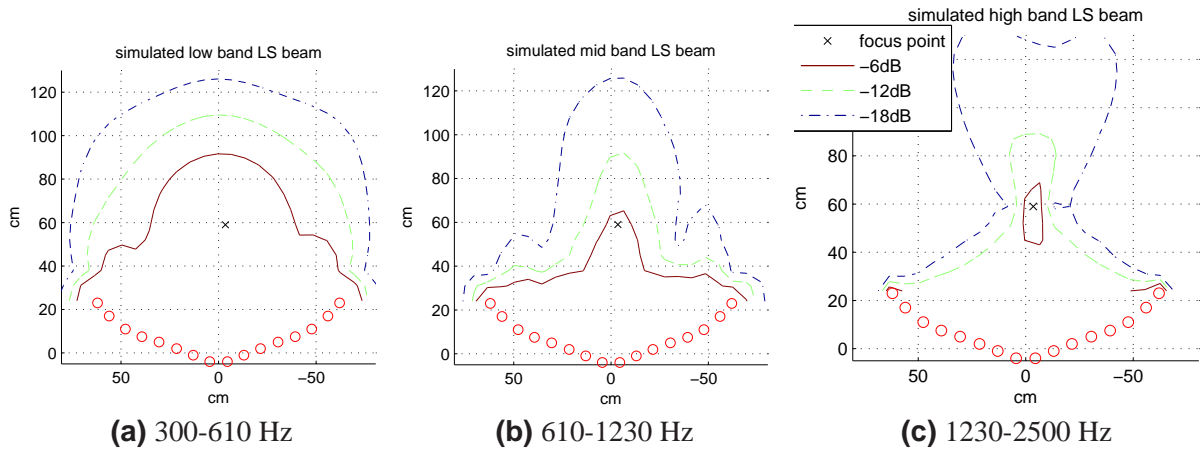


**Figure B.2:** Least squares beam. The beam has a steep decay towards the back.

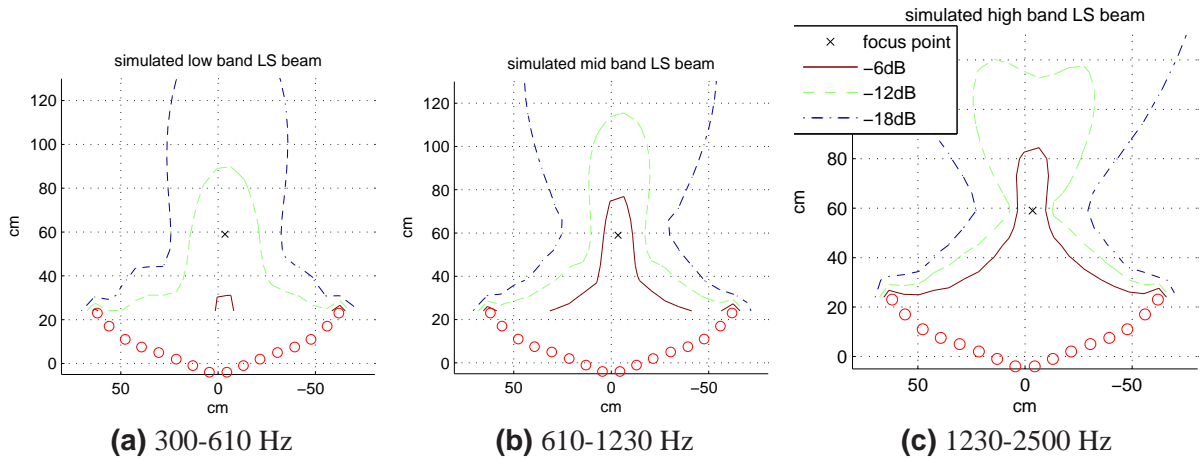


**Figure B.3:** LSB with SVD regularization. There is a shift of weights to the high frequencies. The beam is still narrow, but does not decay as fast towards the rear end as the LSB without regularization.

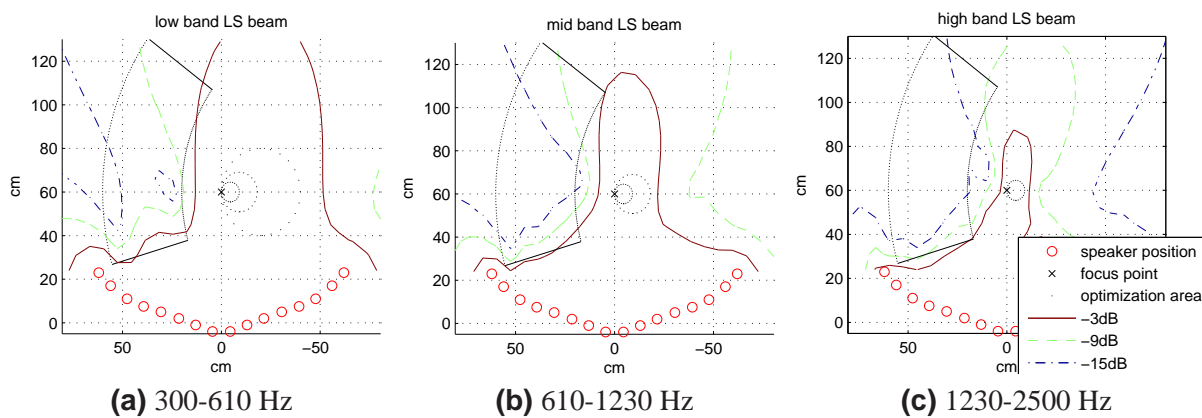


**Figure B.4:** LSB with frequency dependent focus area. The size of the focus area decreases with the frequency. Low frequencies are therefore stronger weighted.

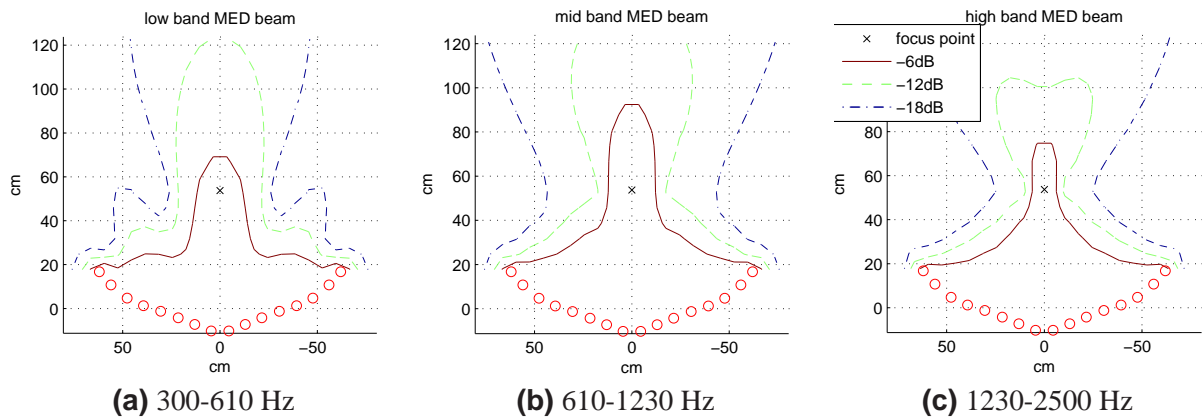


**Figure B.5:** MED beam. The tuning factor  $\alpha$  was set to get a trade off between the WDSB and the LSB. There is a suppression of low frequencies, but not as strong as for the LSB with SVD.

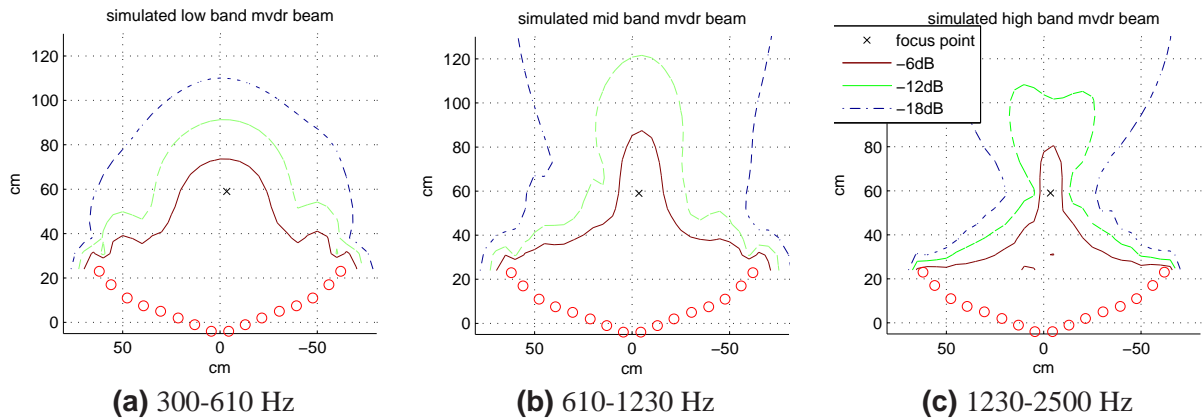


**Figure B.6:** MVDR beam. Like the LSB, the MVDRB has a steep decay towards the rear end at low frequencies. In the upper frequency bands, it does not perform as well as the LSB, because it has the constraint of unity gain in the focus point.

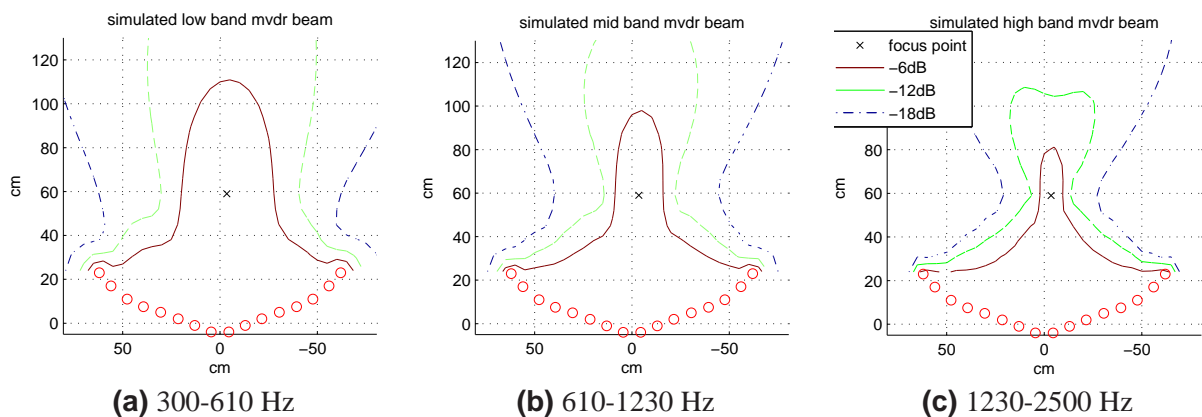
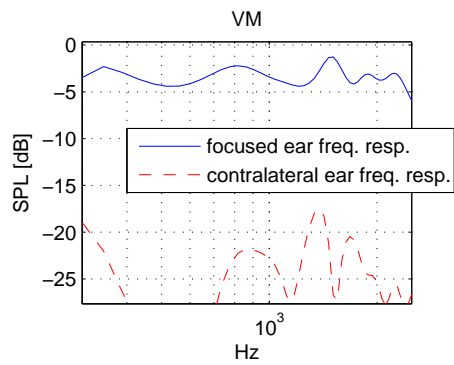


**Figure B.7:** MVDR with SVD regularization. The beam loses its steep decay towards the end at low frequencies, but it is still narrower than the WDSB.

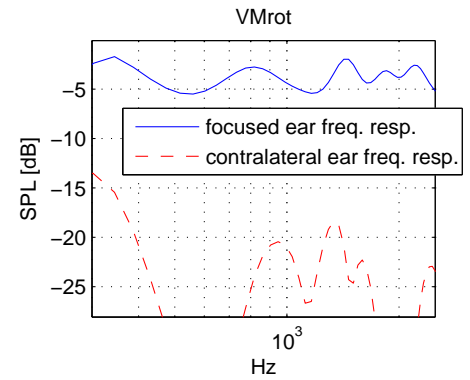
# Appendix C

## XTC Frequency Responses

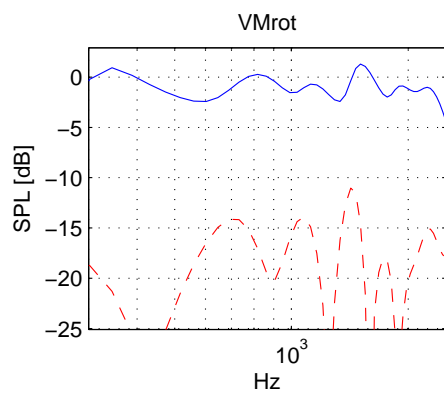
The cross talk of the transaural beamformer was measured in four positions with  $0^\circ$  and  $30^\circ$  head rotation each. These positions are marked in Fig.3.7. The frequency responses of these measurements are presented in the following.



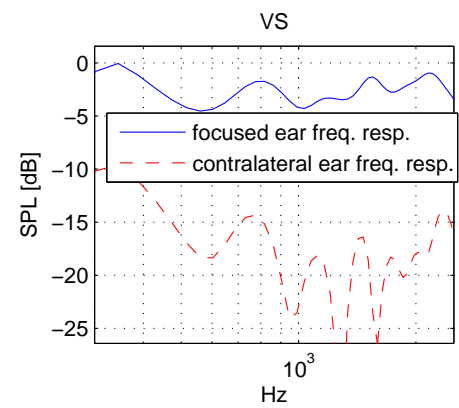
(a) Close central position.



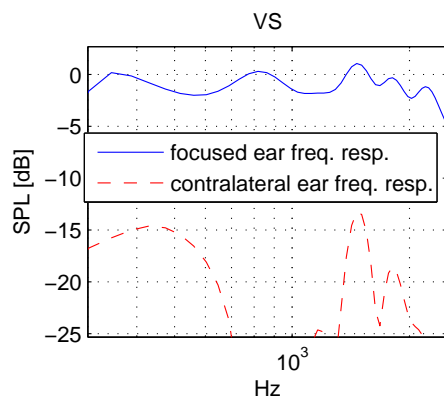
(b) Close central position 30° rotation.



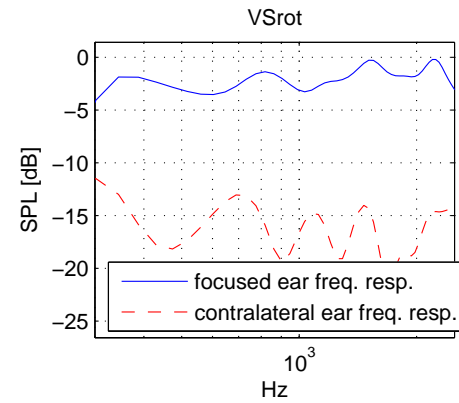
(c) Close central position 30° rotation.



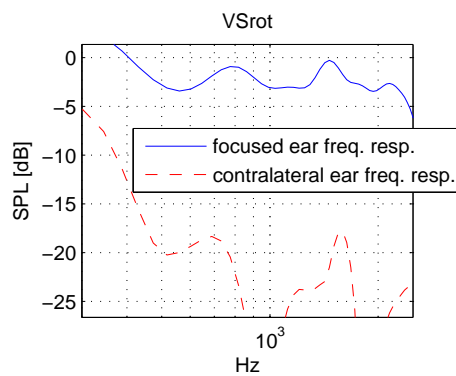
(d) Close side position.



(e) Close side position.

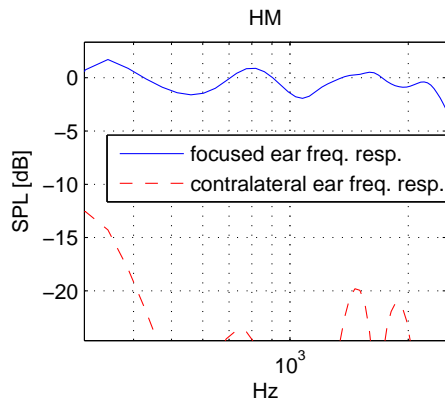


(f) Close side position 30° rotation.

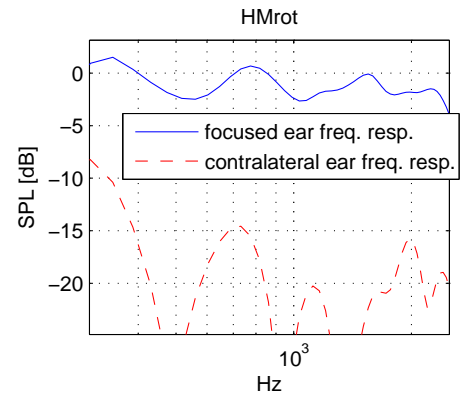


(g) Close side position 30° rotation.

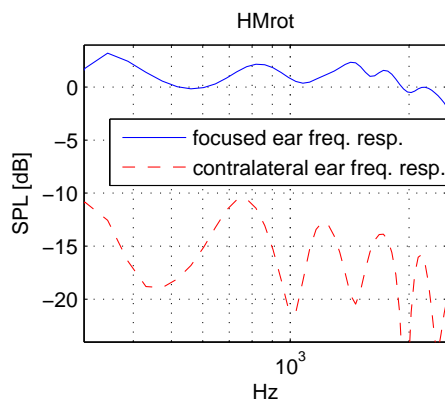
**Figure C.1:** XTC frequency responses for the close head positions, marked in Fig.3.7.



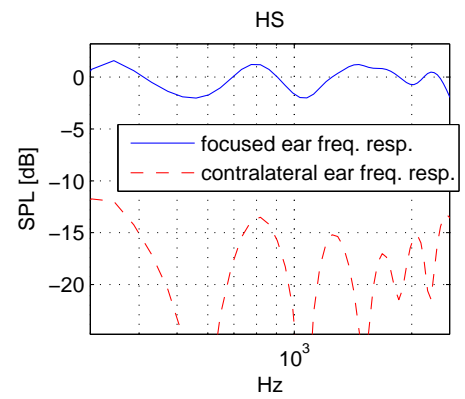
(a) Rear central position.



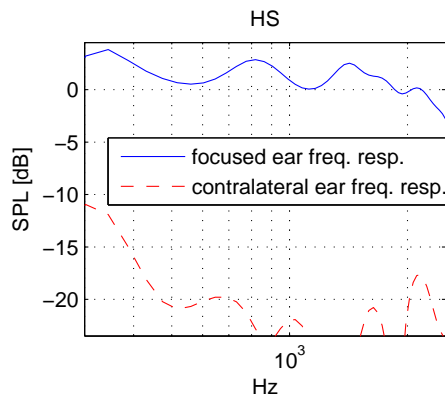
(b) Rear central position 30° rotation.



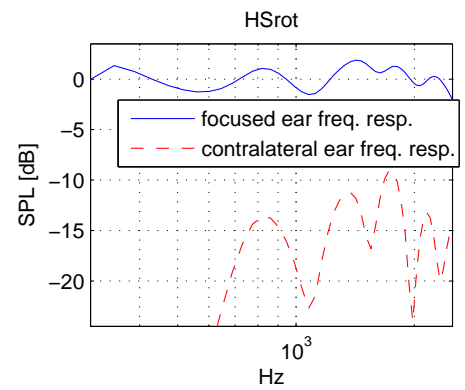
(c) Rear central position 30° rotation.



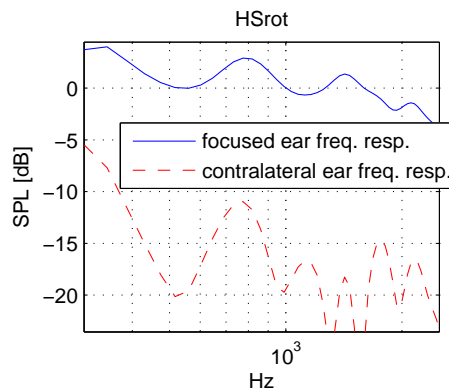
(d) Rear side position.



(e) Rear side position.



(f) Rear side position 30° rotation.



(g) Rear side position 30° rotation.

Figure C.2: XTC frequency responses for the rear head positions, marked in Fig.3.7.

# Bibliography

- Ahnert, W. (1993). *Beschallungstechnik; Grundlagen und Praxis*. Stuttgart [u.a.].
- Algazi, V. R., Avendano, C., and Duda, R. O. (2001). Estimation of a spherical-head model from anthropometry. *JOURNAL- AUDIO ENGINEERING SOCIETY*, 49:472–479. ID: 208781859.
- Atal, B. S. and Schroeder, M. R. (1963). Computer simulation of sound transmission in rooms. In *IEEE Conv. Record*, pages 150–155.
- Bai, M. R., Tung, C.-W., and Lee, C.-C. (2005). Optimal design of loudspeaker arrays for robust cross-talk cancellation using the taguchi method and the genetic algorithm. *J. Audio Eng. Soc.*, 117(5):2802–2813.
- Bauck, J. and Cooper, D. H. (1996). Generalized transaural stereo and applications. *J. Audio Eng. Soc.*, 44(9):683–705.
- Blauert, J. (1999; 1999). *Spatial hearing; The psychophysics of human sound localization*. MIT Pr., Cambridge, Mass. [u.a.].
- Brandstein, M. and Ward, D. B., editors (2001). *Microphone arrays : signal processing techniques and applications*. Springer, Beerlin ; London.
- Cho, Y. T. and Roan, M. J. (2009). Adaptive near-field beamforming techniques for sound source imaging. *The Journal of the Acoustical Society of America.*, 125(2):944. ID: 302066175.
- Domínguez, A. C. (2009). Pre-processing of speech signals for noisy and band-limited channels. Master's thesis, School of Electrical Engineering, Kungliga Tekniska Högskolan, Stockholm, Sweden.
- Farina, A. (2000). Simultaneous measurement of impulse response and distortion with a swept-sine technique. In *108th AES Convention*, pages 18–22.
- Fasold, W. (1998). *Schallschutz und Raumakustik in der Praxis; Planungsbeispiele und konstruktive Lösungen*. Verl. für Bauwesen.



- Gardner, W. G. (1997). Head tracked 3-d audio using loudspeakers. In *IEEE Workshop on Applications of Signal Processing to Audio and Acoustics*, New York, USA.
- Guldenschuh, M. and Sontacchi, A. (2009). Transaural stereo in a beamforming approach. In *DAFx-09*.
- Guldenschuh, M., Sontacchi, A., Zotter, F., and Höldrich, R. (2008). Principles and considerations to controllable focused sound source reproduction. In *7th Eurocontrol INO Workshop*.
- Keele, D. B. (2003). Full-sphere sound field of constant-beamwidth transducer (cbt) loudspeaker line arrays. *JOURNAL- AUDIO ENGINEERING SOCIETY*, 51:611–624. ID: 208876013.
- Kirkeby, O. and Nelson, P. A. (1999). Digital filter design for inversion problems in sound reproduction. *JOURNAL- AUDIO ENGINEERING SOCIETY*, 47(7/8):583–595. ID: 210604884.
- Laumann, K., Theile, G., and Fastl, H. (2008). A virtual headphone based on wave field synthesis. In *Acoustics 08 Paris*, pages 3593–3597, Paris, France.
- Lentz, T. (2006). Dynamic crosstalk cancellation for binaural synthesis in virtual reality environments. *J. Audio Eng. Soc.*, 54(4):283–295.
- Mabande, E. and Kellermann, W. (2007). Towards superdirective beamforming with loudspeaker arrays. In *Conf. Rec. International Congress on Acoustics*, Madrid, Spain.
- Mabande, E., Schad, A., and Kellerman, W. (2009). Robust superdirectional beamforming for hands-free speech capture in cars. In *NAG/DAGA 2009*, Rotterdam, NL.
- Menzel, D., Wittek, H., Theile, G., and Fastl, H. (2005). Binaural sky: A virtual headphone for binaural room synthesis. In *Tonmeistersymposium 2005*, Hohenkammer, Germany.
- Moller, H., Sorensen, M. F., Hammershoi, D., and Jensen, C. B. (1995). Head-related transfer functions of human subjects. *Journal of the Audio Engineering Society.*, 43(5):300. ID: 87542869.
- Moore, B. C. (1995). *Hearing*, chapter Frequency Analysis and Masking, pages 161–206. Academic Press, San Diego, USA / London, UK.
- Morse, P. M. (1953). *Methods of theoretical physics*. McGraw-Hill Book Co, New York ; London.
- Möser, M. (1988). *Analyse und Synthese akustischer Spektren*. Berlin [u.a.].
- Noisternig, M., Sontacchi, A., Musil, T., and Höldrich, R. (2003). A 3d ambisonics based binaural sound reproduction system. In *24th international AES Conference: Multichannel Audio*.

- Oppenheim, A. V. (1989). *Discrete-time signal processing*. Prentice-Hall, Englewood Cliffs, NJ [u.a.].
- Schäfer, F. (2008). Artificial bandwidth extension of narrowband speech. Master's thesis, Graz University of Technology, Graz, Austria.
- Shin, M., Lee, S. Q., Kim, D., Wang, S., Park, K. H., Fazi, F. M., Nelson, P. A., and Seo, J. (2009). Maximization of acoustic energy difference between two spaces. *to be published*.
- Veen, B. D. V. and Buckley, K. M. (1988). Beamforming: a versatile approach to spatial filtering. *ASSP Magazine, IEEE*, 5; 5(2):4–24. ID: 1.
- Williams, E. G. (1999). *Fourier acoustics; Sound radiation and nearfield acoustical holography*. Academic Press, London [u.a.].
- Yon, S., Tanter, M., and Fink, M. (2003). Sound focusing in rooms: The time-reversal approach. *The Journal of the Acoustical Society of America.*, 113(3):1533. ID: 96597221.
- Zwicker, E. (1990). *Psychoacoustics; Facts and models*. Berlin [u.a.].